Journal of Alloys and Compounds 883 (2021) 160727

Contents lists available at ScienceDirect

Journal of Alloys and Compounds

journal homepage: www.elsevier.com/locate/jalcom

Review

A review of low-dimensional metal halide perovskites for blue light emitting diodes

Xiaodong Peng[1], Cheng Yan[1], Fengjun Chun, Wen Li, Xuehai Fu, Weiqing Yang*

Key Laboratory of Advanced Technologies of Materials (Ministry of Education), School of Materials Science and Engineering, Southwest Jiaotong University, Chengdu 610031, PR China

ARTICLE INFO

Article history:
Received 9 March 2021
Received in revised form 31 May 2021
Accepted 3 June 2021
Available online 6 June 2021

Keywords:
Low-dimensional metal halide perovskites
Quantum dots
Nanoplatelets
Quasi-2D perovskites
Blue light emitting diodes

ABSTRACT

Low-dimensional metal halide perovskites (LMHPs) hold promising potential for light emitting diodes due to high color purity, strong exciton binding energy, and facile film fabrication of the emitting layer. However, in contrast with red and green counterparts, blue light emitting diodes (LEDs) still encounter some tough problems in efficiency, luminance, and operational stability. In recent years, dramatically increasing investigations have been devoted to the synthesis method of LMHPs for blue LEDs. Herein, we describe the recent advances on blue low-dimensional perovskites involving zero-dimensional quantum dots (0D QDs), two-dimensional nanoplatelets (2D NPLs), and quasi-two-dimensional perovskites (quasi-2D perovskites) as well as the related devices. Further, we provide a new perspective for the development of blue-emissive perovskite LEDs in industrialization, including the strategies for improving performance and solutions for major challenges regarding deep-blue perovskite LEDs.

Contents

1. Introduction

As the emerging semiconductor material, metal halide perovskite is considered as a promising candidate for low-cost, large-area and high-efficiency optoelectronic devices, especially LEDs [1–5]. Usually, metal

* Corresponding author.
E-mail address: wqyang@swjtu.edu.cn (W. Yang).
[1] These authors contributed equally to this work.

https://doi.org/10.1016/j.jallcom.2021.160727
0925-8388/

halide perovskite possesses a chemical formula of ABX_3, where A-site represents a monovalent organic or inorganic cation, e.g., $CH_3NH_3^+$ (MA^+), $CH(NH_2)_2^+$ (FA^+), Cs^+ ; B-site is a divalent metal cation, e.g., Pb^{2+}, Cu^{2+}, Sn^{2+}; X-site is a halide anion, e.g., Cl^-, Br^- and I^-. Low-dimensional metal halide perovskites (LMHPs) have been largely explored and applied in optoelectronic devices due to their superiorly quantum-confined optical characteristics such as narrow emission bandwidth, strong defect tolerance ability, easily tunable emission wavelength, and high photoluminescence quantum yield (PLQY) [6–10]. LMHPs, including 0D QDs, 2D NPLs, as well as quasi-2D perovskites, are referring to perovskite crystals with at least one reduced dimension which satisfies the condition of quantum confinement effect. Generally, the electron-hole pairs in three-dimensional (3D) perovskites have the smaller binding energy, indicating that excitons can easily dissociate into free carriers. However, free carriers can be readily captured by trap states leading to non-radiative recombination, which is unfavorable to luminescent devices [1,11]. Contrastively, LMHPs possess the higher radiative excitonic recombination in comparison with 3D perovskites at room temperature due to the high charge-carrier densities and the strong exciton binding energies up to hundreds of millielectronvolts (meV) [12,13]. Besides, the ionic defects are inevitably formed in the polycrystalline thin films based on 3D halide perovskite owing to the high ionic mobility in crystallization process. LMHPs are prepared in a single-crystalline state resulting in the related spin-coated emissive film shows higher crystallinity with fewer ionic defects than conventional bulk 3D perovskite film in the fabrication of LEDs [14–16].

Currently, green-, red- and near-infrared- emissive perovskite light emitting diodes (PeLEDs) have achieved huge successes, of which external quantum efficiency exceed 20%, reaching up to 23.4% [17], 21.3% [18], and 21.6% [19], respectively. Nevertheless, as one of the three primary colors, blue PeLEDs still lag behind the red and green PeLEDs [20]. In this regard, Kumawat et al. [21] prepared blue PeLEDs using 3D $CH_3NH_3PbBr_{1.08}Cl_{1.92}$, whereas limited external quantum efficiency (EQE) values-(≈ 0.0003%) were achieved. Fortunately, Zeng's group [9] reported a blue LED based on low-dimensional nanocrystals, showing a higher EQE of 0.07% and a maximum current efficiency of 0.14 cd A^{-1} at a brightness of 742 cd m^{-2}. This work opened a way for the blue PeLEDs by using low-dimensional nanostructures. Subsequently, Huang's group explored the quasi-2D perovskite film for the fabrication of sky-blue LEDs [22]. Since then, LMHPs have received considerable attention for improving the performance of blue-emitting PeLEDs. Especially in 2019 and 2020, striking progress have been demonstrated in both efficiency and luminance for the LMHPs-based blue PeLEDs but they still fall behind red and green LEDs. Notably, the representative LMHPs as well as the correlative LEDs are presented in Fig. 1.

In this review, we highlight the recent advances on blue low-dimensional perovskites involving colloidal 0D QDs, colloidal 2D NPLs, and quasi-2D perovskites as well as the related PeLEDs. Also, we discuss the future research directions for propelling the development of blue PeLEDs, including the strategies for improving performance and solutions for major challenges about deep-blue PeLEDs in detail.

2. 0D colloidal perovskite QDs for blue emission

2.1. Pure bromide-based QDs

The strong quantum confinement effect gives rise to expanded bandgap in perovskites when the size of nanoparticles is smaller than exciton Bohr radius [23]. In comparison to stable green QDs (e.g., Cs/MA/FA$PbBr_3$), pure bromide-based QDs with the smaller size under Bohr radius have the wider bandgaps located in the blue-emissive range. For instance, it is reported that the exciton Bohr radius of bulk $CsPbBr_3$ is around 7 nm [24], implying that the size of blue-emitting QDs should be reduced to 7 nm. However, ultra-small QDs are prone to agglomeration, making the preparation of ultra-small-sized QDs a relatively difficult process. Colloidal perovskite nanoparticles can be synthesized using two

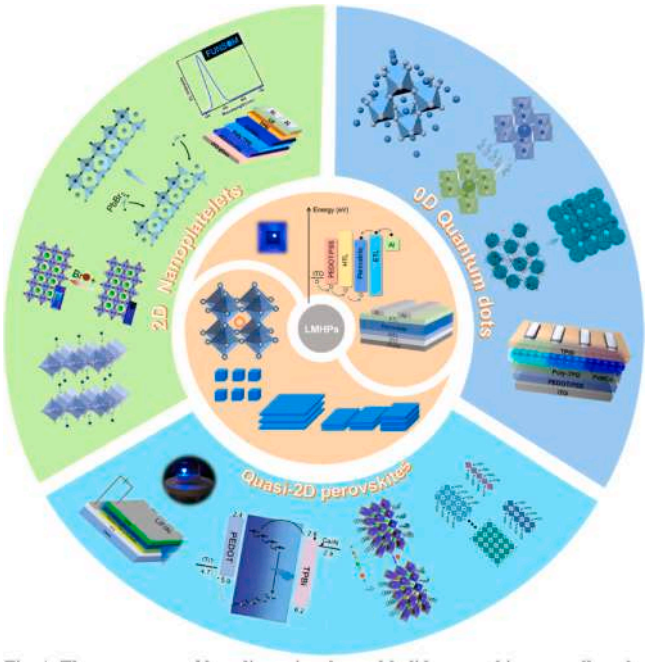

Fig. 1. The represents of low-dimensional metal halide perovskites as well as the related blue LEDs. The part of 0D quantum dots (QDs): Structure diagram of QDs; B-site doped QDs [34] Copyright 2017, American Chemical Society; Ligand-exchange engineering [29] Copyright 2020, Springer Nature; Device architecture [80] Copyright 2019, American Chemical Society. The part of 2D nanoplatelets (NPLs): Structure diagram of NPLs [2] Copyright 2020, Wiley-VCH; In situ passivation for modification of NPLs [68] Copyright 2018, American Chemical Society; Defect repairing by $PbBr_2$-ligand solution [67] Copyright 2018, American Chemical Society; Device architecture and EL spectra [64] Copyright 2018, Elsevier Science Inc. The part of quasi-2D perovskites: Structure diagram of quasi-2D perovskites [105] Copyright 2019, Springer Nature; A-site doping for high-performance devices [121] Copyright 2020, Springer Nature; Schematic diagram of band and working mechanism based on quasi-2D devices [110] Copyright 2020, Wiley-VCH; Device architecture with a working photograph [109] Copyright 2019, Springer Nature. (Note: description in a clockwise direction).

methods: ligand-assisted reprecipitation and hot-injection method (Note: the hot-injection method will be described in detail in Section 2.3). The ligand-assisted reprecipitation method via supersaturated crystallization is simple and convenient. Particularly, the precursor in a polar solvent (e.g., N, N-dimethylformamide (DMF), dimethyl sulfoxide (DMSO)) containing organic ligands is added dropwise into a nonpolar solvent (e.g., toluene, n-hexane). The colloidal perovskite nanoparticles can be prepared immediately due to the difference in solubility of precursor between two solvents. By changing the synthesis temperature of ligand-assisted reprecipitation, Song's group [25] prepared blue-emission $CsPbBr_3$@SiO_2 nanospheres with a 2.8 nm average particle size, demonstrating 72% PLQY and good stability under the protection of the SiO_2 shell. Later, Wang et al. [26] obtained core-shell structured $CsPbBr_3$@amorphous $CsPbBr_x$ blue-emitting QDs through the hot injection method, which showed the higher PLQY up to 84% (Fig. 2a, b). Although equipped with satisfactory luminescent efficiency, the reason for the high PLQY of the ultra-small perovskite QDs was hazily explored. Fortunately, Li et al. [27] reported ultra-small (~ 3 nm) $CsPbBr_3$ QDs exhibiting 12.4 nm of narrow full width at half maximum (FWHM) with 68% PLQY. They found that high PLQY in ultra-small QDs is closely related to the high-density band tail states that promote the relaxation of photocarriers, inducing greater possibility for radiative recombination. As is shown in Fig. 2c, in addition to directly radiative recombination upon above-gap excitation (process II), the photocarriers generated by sub-gap excitation (process I) can hop into the extended states, and then the trapped carriers' transit between lower and high energy levels in band tail states. Subsequently, the relaxed carriers in tail states can

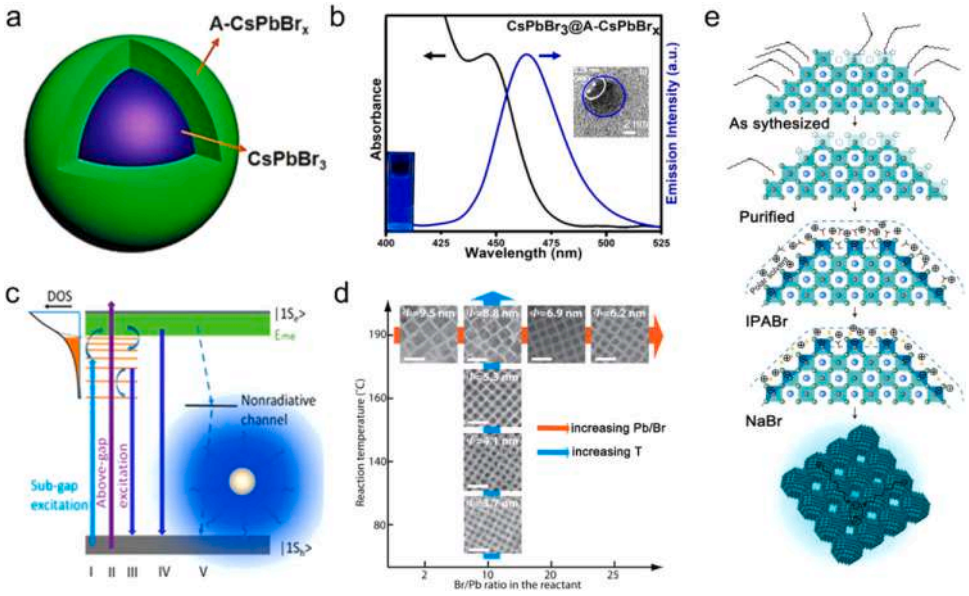

Fig. 2. Pure bromide-based quantum dots (QDs). (a) The core-shell structured $CsPbBr_3$@amorphous $CsPbBr_x$ QDs. (b) PL and absorption spectra of $CsPbBr_3$@amorphous $CsPbBr_x$ QDs. Reprinted with permission [26]. Copyright 2018, American Chemical Society. (c) The mechanism of photocarrier dynamics in the ultra-small QDs. Reprinted with permission [27]. Copyright 2017, American Chemical Society. (d) Controlling the shape and size of QDs by tuning the temperature and Br-to-Pb ratio, respectively. Reprinted with permission [28]. Copyright 2018, American Chemical Society. (e) The synthesis process of bipolar-shell structured QDs. Reprinted with permission [29]. Copyright 2020, Springer Nature.

recombine radiatively (process III), resulting in PLQY enhancement of ultra-small QDs.

Indeed, small-sized QDs severely suffer from inferior uniformity which causes low color purity with a wide FWHM. To address this issue, Son's group [28] reported a greatly effective method for tuning the size of $CsPbX_3$ QDs with perfect uniformity based on thermodynamic equilibrium. The $CsPbBr_3$ QDs of several sizes were synthesized by adjusting the Br-to-Pb ratio and the reaction temperature. As shown in Fig. 2d, as the Br-to-Pb ratio increases, the QD size decreases at a certain temperature, exhibiting a more uniform distribution. Simultaneously, at a constant Br-to-Pb ratio, the size of QDs is inversely correlated with temperature. Most recently, Sargent's group [29] proposed bipolar-shell resurfacing modulation to prepare blue $CsPbBr_3$ QDs (4 nm) with an unexpected PLQY value of 91%. To achieve bipolar-shell structured nanocrystals, isopropylammonium bromide (IPABr) was introduced into purified QDs solution to form a rich-bromine surface, and then NaBr was added to replace most organic ligands to reduce electronic and hole injection barriers (Fig. 2e).

Though ultra-small pure-bromide QDs possess high PLQY and good stability with some protective shell, it is difficult to prepare small QDs with high ensemble uniformity and narrow FWHM. Unless these obstacles are solved, the 0D bromine-based QDs will be hard to apply in optoelectronic applications.

2.2. B-site doped QDs

Commonly, the energy band structure of perovskite (ABX_3) mainly depends on B-site and X-site atoms. The valence band is determined by the outermost *s* orbital of the B-site metal ion and the *p*-orbitals of the X-site halogen atoms, while the conduction band is composed of the outermost *p* orbitals of metal ions (Fig. 3a). As a result, doping other atoms into perovskite crystals (ABX_3) could always provide a virtual way to tune bandgap and stabilize perovskite crystal structure effectively [30]. Notably, A-site cations doping does not dramatically alter the perovskite bandgap but does improve phase stability [31]. $CsPbI_3$, for example, has a small tolerance factor (t) which is related to perovskite structural stability due to smaller Cs^+ cations, causing the transformation of cubic structure into the asymmetric orthorhombic structure. FA-doped $CsPbI_3$ nanocrystals show better chemical durability and a more stable phase structure with higher quantum yields than pure $CsPbI_3$ nanocrystals [32]. However, B-site doping directly tunes the bandgap of QDs to extend the spectrum to the blue region. The radius and electronic configuration of doped atoms should be similar to that of lead atoms for B-site doping blue-emissive QDs, because only these atoms can form the similar bond energy with halogen atom compared to Pb—X bond, involving Bi^{3+}, Mn^{2+}, Sn^{2+}, Zn^{2+}, Cu^{2+}, Cd^{2+}, Al^{3+}, etc. [31].

It is more effective to partially substitute Pb-site for band engineering, which is accomplished by adjusting the bandgap or introducing a new energy level. Specifically, some B-site dopants, such as Cd^{2+}, may escape from the perovskite octahedral lattice which easily leads to their emission color shifting from blue to green [33]. Excessive dopants can cause malignant emissions. For example, undesirable Mn^{2+} doping could generate yellow emissions. Therefore, reasonable dopants and optimal doping concentrations are crucial for doped blue-emitting perovskites. Ward et al. [34] reported that cation exchange reactions take place in $CsPbBr_3$ nanocrystals by replacing Pb^{2+} with divalent cations (M = Cd^{2+} and Zn^{2+}), as illustrated in Fig. 3b. The Pb^{2+} for M^{2+} cation exchange results in a hypsochromic shift of emission spectrum as well as the absorption while preserving the relatively high PLQY (> 50%) and narrow PL FWHM (80 meV) compared with pristine nanocrystals. This blue-shift phenomenon is attributed to the contraction of the perovskite cubic crystals, owing to short Pb—X bonds and strong ligand fields within the lead-halide octahedral. Elsewise, a doping impurity may form a new energy level, which has an obvious influence on optical properties [35]. Liu et al. proposed Al^{3+}-doped $CsPbBr_3$ (Al: $CsPbBr_3$) with stable blue photoluminescence via hot injection, with $AlBr_3$ serving as the impurity precursor [36]. After Al doping into the perovskite crystal lattice, the green luminescence spectrum (515 nm) of $CsPbBr_3$ nanocrystals was shifted to a deep-blue spectrum (456 nm) of Al: $CsPbBr_3$ nanocrystals (Fig. 3c). Combining with theoretical calculation, the results revealed that Al doping introduces a new level in the bandgap originating from the hybridization of Al *s*-orbitals, Br *p*-orbitals and the Pb *p*-orbitals.

In addition to partially replacing the lead atoms at the B position, the lead atoms are entirely replaced to form a lead-free blue luminescent perovskite. Lead halide perovskites have better

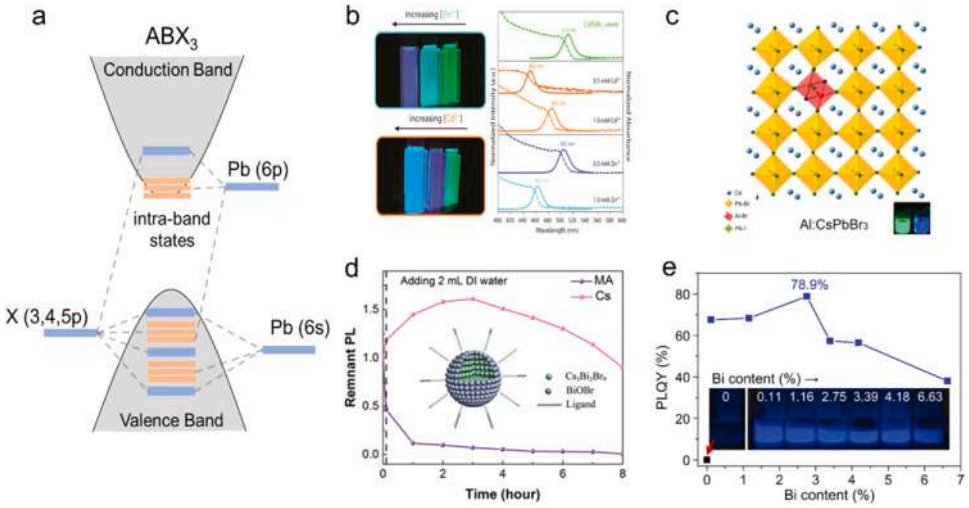

Fig. 3. B-site doped quantum dots (QDs). (a) Energy band structure of bulk perovskite. (b) The photoluminescence spectra and UV-illumination photographs of doped $CsPbBr_3$ QDs by Cd^{2+} and Zn^{2+} bromide salts. Reprinted with permission [34]. Copyright 2017, American Chemical Society. (c) Lattice diagram and inserted photograph under UV irradiation of Al^{3+}-doped $CsPbBr_3$. Reprinted with permission [36]. Copyright 2017, Wiley-VCH. (d) Schematic diagram of stability test in deionized water for $Cs_3Bi_2Br_9$ QDs compared with $MA_3Bi_2Br_9$. Insets: the structure of $Cs_3Bi_2Br_9$ QDs passivated by BiOBr shell [38]. Reprinted with permission. Copyright 2018, Wiley-VCH. (e) PLQY of Cs_2SnCl_6: x% Bi with a series of different concentrations of Bi. Inset represents the pictures of Cs_2SnCl_6: x% Bi under 365 nm UV illumination. Reprinted with permission [39]. Copyright 2018, Wiley-VCH.

optoelectronic properties than lead-free halide perovskites, but they still have certain drawbacks, such as poor environmental stability and heavy metal lead toxicity. Thus, lead-free LMHPs are supposed to be potential luminescent materials, especially for blue emission. Recently, tin-based and bismuth-based lead-free perovskite QDs have been investigated. In 2018, Leng and co-workers [37] prepared $MA_3Bi_2Br_9$ QDs that exhibited a PLQY of 54.1% at 422 nm after Cl^- anions surface passivating but encountered crystal collapse. Based on their previous work, they further explored all-inorganic Bi-based perovskite QDs ($Cs_3Bi_2Br_9$ QDs) at a wavelength of 410 nm with a PLQY of 19.4% [38]. $Cs_3Bi_2Br_9$ QDs outperformed $MA_3Bi_2Br_9$ QDs in terms of photostability and moisture stability, owing to surface passivation by the BiOBr shell (Fig. 3d). For Sn-based lead-free perovskites, Tan et al. [39] improved quantum efficiency up to 78.9% in blue-emitting perovskites (Fig. 3e). To explore the mechanism of blue photoluminescence of Bi-doped Cs_2SnCl_6, they illustrated that photoluminescence originated from donor-acceptor pair emission of two defects ascribing to the $Bi_{Sn} + V_{Cl}$ defect complex. The effective B-site doping can not only realize blue luminescence, but also passivate some surface defects by remaining impurity. Furthermore, due to their environment-friendly low toxicity, lead-free perovskites are likely to become research hotspots for PeLEDs in the future.

2.3. Mixed halide nanocrystals

In addition to small-size pure bromide-based LMHPs for blue emission, mixing halide anions is another way to get blue spectral emission owing to the perovskites' strong halogen anion exchange [40]. Fig. 4a shows that the mixed halide perovskite nanocrystals (NCs) can cover the entire visible light spectrum range by varying

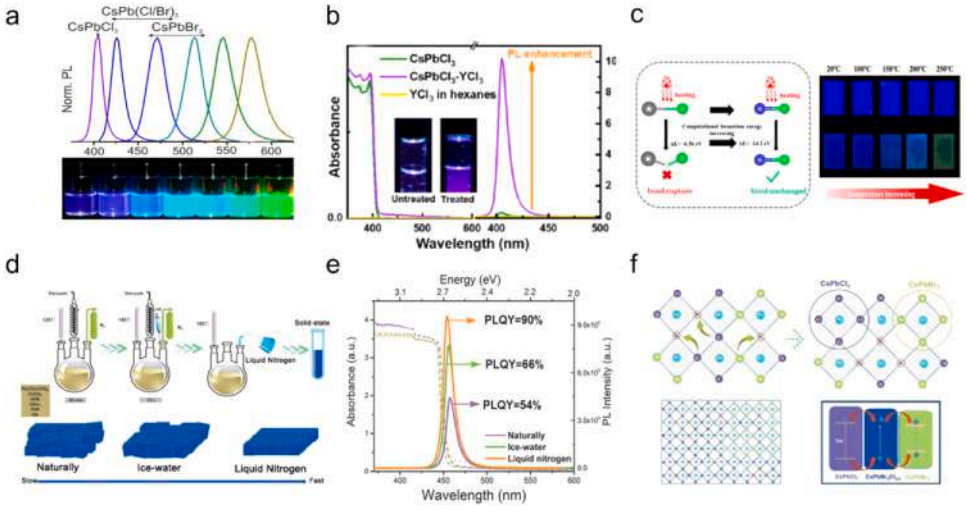

Fig. 4. Mixed halide nanocrystals (NCs). (a) PL spectra of Cl^-/Br^- mixed nanocrystals and photographs of colloidal $CsPb(Br_xCl_{1-x})_3$ solutions under UV illumination. Reprinted with permission [41]. Copyright 2015, American Chemical Society. (b) Ultraviolet absorption and PL spectra for pristine $CsPbCl_3$ NCs and YCl_3-passivated $CsPbCl_3$ NCs. Insets are pictures of pristine samples and optimized samples by YCl_3 under 365 nm ultraviolet radiation. Reprinted with permission [50]. Copyright 2018, American Chemical Society. (c) The left half of diagram illustrating the formation energies of Pb—Br and Cu—Br bond. The Photographs on right side showing various emissions of nanocrystals deposited films at increasing annealing temperature for doped $CsPb(Br_xCl_{1-x})_3$ with Cu^{2+} and without it. Reprinted with permission [52]. Copyright 2019, American Chemical Society. (d) Schematics of the ultrafast thermodynamic control strategy and (e) PL spectra with corresponding PLQY at different cooling rates for $CsPbBr_xCl_{3-x}$ NCs. (f) Microscopic model of ion migration and phase segregation for $CsPbBr_xCl_{3-x}$ NCs. Reprinted with permission [57]. Copyright 2020, Wiley-VCH.

proportions of halide anions, which means that the blue spectrum range can be obtained by controlling the concentration ratio between Br^- and Cl^- [41]. In 2015, the blue-emissive mixed halide perovskites ($MAPbBr_{1.08}Cl_{1.92}$) were successfully applied to light-emitting diodes [21]. Since then, substantive studies have focused on preparing highly efficient mixed halide perovskites which could be one of the most promising candidates for blue light-emitting diodes [9,42–44].

Typically, conventional ligands such as oleylamine (OAm) and oleic acid (OA) are usually used to moderate the mixed halide nanocrystals. It is reported by Roo et al. that the OAm and OA have weak interactions with perovskite surfaces owing to highly dynamic dissociation [45]. Therefore, substituting other available ligands for conventional ligands is an effective way to stabilize nanostructure and facilitate carrier transport under blue LED operating conditions. Based on fast halogen anion exchange, the blue-emitting $CsPbBr_xCl_{3-x}$ NCs can be facilely obtained through combining as-prepared $CsPbCl_3$ NCs and $CsPbBr_3$ NCs solution. It is well known that $CsPbBr_3$ NCs possess a high PLQY and excellent defect tolerance, while $CsPbCl_3$ NCs with a low PLQY usually are susceptible to ion migration with the formation of deep-trap states [30]. $CsPbCl_3$ is highly vulnerable to defects due to its low defect resistance, resulting in deplorable PLQY. The Cl vacancy defects in mixed halide perovskite NCs can promote the creation of deep energy levels within the valence band and conduction band during the crystallization process, leading to non-radiative recombination channels. Hence, it is important to passivate Cl vacancy defects in $CsPbCl_3$ NCs before mixing $CsPbBr_3$ NCs and $CsPbCl_3$ NCs in attempts to obtain high quality blue-emitting $CsPbBr_xCl_{3-x}$ NCs.

Many optimization strategies were carried out to improve the PLQY and suppress phase segregation, such as ligand exchange [46–49], inorganic halide salts passivation [50,51], doping impurity atoms [44,52,53], and so on. The ligand exchanging and doping strategies will be further discussed in the following device-based chapter because they could distinctly improve the performance of LEDs. Organic ligands can indeed stabilize the $CsPbBr_xCl_{3-x}$ NCs but they also have some negative effects in LEDs, such as insulating barriers and poor electroluminescence properties [54]. As a comparison, inorganic halide salts not only fully passivate defects but also reduce the negative effects caused by organic ligands. Furthermore, trivalent metal halide salts have been proven to passivate defect traps effectively. Ahmed et al. [50] firstly demonstrated the halide salts passivation can bring remarkable enhancement in the PLQYs of $CsPbCl_3$ NCs of up to 60% (Fig. 4b). They further explored the dual-surface passivation of $CsPbCl_3$ NCs, finding that YCl_3 passivation would not only preserve the size and structure of inherent NCs, but also compensate for Pb-Cl ion vacancies on the surface, effectively meliorating surface trap states and suppressing the non-radiative recombination. On the basis of previous research, our group devised a new $PrCl_3$ pre-passivation strategy for blue-emitting $CsPbBr_xCl_{3-x}$ NCs [51]. Through fast halogen anion exchange, the pre-optimizing $CsPbCl_3$ NCs were mixed into $CsPbBr_3$ to obtain blue-emitting $CsPbBr_{1.5}Cl_{1.5}$ NCs with a nearly 7-fold notable improvement in PLQY from 13% to 89%. Perovskites, as we all know, are extremely unstable in a moderately high-temperature atmosphere [55,56]. Bi et al. [52] discovered that copper-doped all inorganic $CsPb(Br_xCl_{1-x})_3$ NCs are remarkably thermally stable. As depicted in Fig. 4c, the PLQY of pristine $CsPb(Br/Cl)_3$ NCs decreased to 1% after annealing at 120 °C, while $CsPb_{0.93}Cu_{0.07}(Br/Cl)_3$ NCs remained as high as 35% at 250 °C during the same annealing period, which is attributed to the introducing of Cu—Br bond with high bond energy. In 2015, Kovalenko's group [41] first utilized the traditional hot-injection method to synthesize cesium lead halide perovskites NCs. The $CsPbX_3$(X = I, Br, Cl) NCs are obtained by reacting Cs-oleate with a lead-halide in a three-necked flask at 140–200 °C, and then the mixed solution was cooled down in an ice-water bath. Especially, our group proposed an ultrafast thermodynamic control method via a modified hot-injection method [57]. Unprecedentedly, we changed the cooling rate of nanocrystals in the final stage with liquid nitrogen ultrafast cooling rather than conventional ice water bath cooling (Fig. 4d). Based on the ultrafast thermodynamic control (UTC) strategy, the blue-emitting $CsPbBr_xCl_{3-x}$ NCs have high crystal quality and PLQY (90%) (Fig. 4e). Furthermore, we optimized NCs using $Pb(BrCl)_2$ post-passivation and finally obtained a record-breaking absolute PLQY of 98% with amazing stability of more than 40 h.

Phase segregation hinders the development of blue PeLEDs based on mixed-halide perovskite NCs. Our group proposed a possible guess for phase separation, as shown in Fig. 4f. The presence of inherent halide defects provides a transferable way for adjacent Br^- and Cl^- ions, entailing feasible ion migration under external radiation. Besides, poor crystal quality leads to lattice distortion that may aggravate ion migration as well. As a consequence, the Br-rich and Cl-rich domains are generated during the duration of ion migration. Macroscopically, only the redshift of spectrum can be observed due to charge transfer from wide-bandgap Cl-rich domain to narrow-bandgap Br-rich domain. Therefore, both the passivation of defects and flawless crystal are the key factors for suppressing phase segregation.

3. 2D colloidal pure bromide-based NPLs for blue emission

By reducing the grain size along with the < 100 > crystal orientation to the quantum-confined nanometer size (0.1–2 nm), 2D pure bromide NPLs can achieve blue light emission as well as improved stability along and high exciton binding energy (> 170 meV) (Fig. 5a) [58]. The monolayer thickness of perovskite octahedron is 0.6 nm, which means that the bandgap widens, and the spectra blue shifts noticeably when the number of perovskite layer is less than 4 [59]. According to modification of the reaction condition, like synthesis temperature and concentration of organic cations in the precursor, we can confine the size of 2D NPLs from micro-scale to nanoscale with only a few unit cells thick (n = 1, 2, 3, 4) [60–64].

The colloidal 2D NPLs can be synthesized via ligand-assisted reprecipitation or hot-injection method. As illustrated in Fig. 5b, Urban's group [60] controlled the thickness of the perovskite layer to collect $MAPbBr_3$ NPLs with different optical properties by tuning the ratio of the organic cations (octylammonium bromide) in the reprecipitation process. In their opinion, organic ligands play a critical role in the recrystallization process. Following that, they successfully synthesized 2D $MAPbBr_3$ NPLs with precisely controllable thickness ranging from green emission (n = 7–10) to deep-blue emission (n = 1), exhibiting high PLQYs (40–90%) [61]. Besides, 2D NPLs with varied shapes and thickness could be also prepared by regulating reaction temperature. In 2015, Bekenstein et al. first reported the colloidal $CsPbBr_3$ NPLs [65]. As depicted in Fig. 5c, the reaction temperature at 150 °C produced green-emission symmetrical nanocubes. As the reaction temperature dropped to 130 °C and 90 °C, the resulting perovskite shape changed to lamellar structures with only a few unit cells, presenting blue-shifted PL spectra. Yang et al. [64] proposed that the thickness of ultrathin $CsPbBr_3$ NPLs was precisely controlled at a monolayer level. Strong blue emission was observed in resulting samples by varying reaction time and temperature, and these $CsPbBr_3$ NPLs were successfully applied to light-emitting diodes (Note: This will be mentioned in the subsequent chapter). Gao's group [66] further explored that the amounts of oleic acid (OA) and oleylamine (OAm) in precursors solution will affect the shapes of $CsPbBr_3$ nanocrystals. The separate OA/OAm ratios resulted in bright blue PL emissions at 452 nm, 449 nm, 472 nm and 453 nm with different shapes including 2D nanoplatelets, 2D nanosheets, and 0D quantum dots, respectively. Stranks and co-workers [62] systematically summarized optical properties of these confined NPLs, which could be affected by some factors, including variable cation (Cs^+, $CH_3NH_3^+$, $CH(NH_2)_2^+$) , metal cations (Pb, Sn), halide (Br, I) and thickness (n).

To realize blue emission for pure bromide perovskites, the thickness (n) of NPLs must be reduced to a few layers (n ≤ 4). In general, the thinner the thickness with a higher surface-to-volume ratio, the more

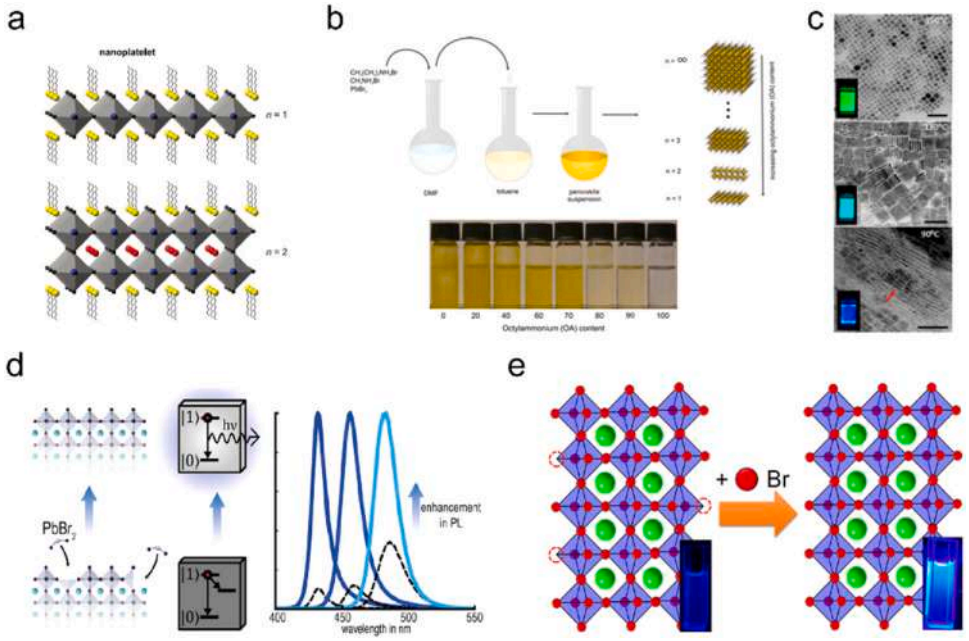

Fig. 5. Pure bromide-based nanoplatelets (2D NPLs). (a) Structure illustration of 2D NPLs of thickness n = 1 and n = 2. Reprinted with permission [62]. Copyright 2016, American Chemical Society. (b) Reprinted with permission [60]. Copyright 2015, American Chemical Society. (c) TEM images showing controlled shapes of $CsPbBr_3$ colloidal perovskites by changing temperature. For reaction temperature, green-emission nanocubes at 150 °C, cyan-emission NPLs at 130 °C, blue-emission at 90 °C. Reprinted with permission [65]. Copyright 2015, American Chemical Society. (d) Post-treatment surface trap repair for boosting blue luminescence by $PbBr_2$-ligand treatment. Reprinted with permission [67]. Copyright 2018, American Chemical Society. (e) In situ passivation of $CsPbBr_3$ dispersions by HBr. Reprinted with permission [68]. Copyright 2018, American Chemical Society.

defects on the surface of NPLs, leading to a significant decrease in PLQYs. Therefore, it is necessary to passivate undesirable defects and modify the nanoplatelet surface. Urban's group [67] presented a novel post-treatment by the addition of a $PbBr_2$-ligand solution to repair halide and lead vacancy. After treatment, the PLQYs of those NPLs markedly rose to 73 ± 2% with spectral region preserved (Fig. 5d). Zeng's group [68] adopted an in situ passivation by adding HBr, which filled the bromide vacancy while also boosted the connection between organic ligands and $PbBr_2$ octahedron. Inspiringly, by introducing the HBr complex solution, the highly blue luminescent $CsPbBr_3$ NPLs were obtained with near 100% absolute quantum yield (98%) (Fig. 5e). Recently, Shamsi et al. [69] employed a short hexylphosphonate ligand ($C_6H_{15}O_3P$) as surface capping ligands in color-pure blue-emitting $CsPbBr_3$ NPLs to significantly suppress these coalescence phenomena. Compared with traditional oleylammonium ligands, short phosphonate ligand (hexylphosphonic acid, HPA) is conducive to forming quantum-confined $CsPbBr_3$ NPLs with favorable stability owing to in-situ surface passivation.

Briefly, there are some ways to obtain colloidal 2D NPLs, such as changing reaction temperature, precursor ratio and ligands content. And the large number of surface defects should be repaired by appropriate passivators.

4. Colloidal 0D QDs and 2D NPLs for blue PeLEDs

According to the difference in relative position of functional layers, the device structure of blue PeLEDs is mainly divided into two types, *p-i-n,* and *n-i-p* architecture (Fig. 6a, b). Under the condition of matched energy level, electrons and holes enter the light-emitting layer via the electron and hole transporting layer to recombine and emit light during the application of the electric field. Generally, the

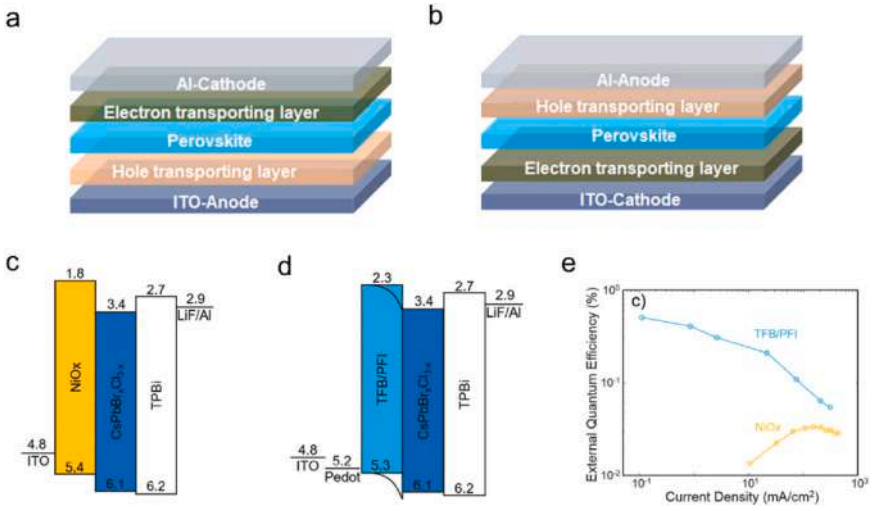

Fig. 6. (a) Schematic drawing of *p-i-n* and (b) *n-i-p* architecture of blue PeLEDs. (c, d) Energy level diagram of the developed LEDs based on NiO_x and TFB/PFI hole transporting layer (e) EQE-current plots for corresponding devices based on NiO_x and TFB/PFI. Reprinted with permission [75]. Copyright 2018, Wiley-VCH.

Table 1
Recent progress of blue PeLEDs based on 0D/2D colloidal LMHPs.

	Perovskites	$EL_{\lambda max}$ (FWHM)/nm	EQE_{max}/%	Devices structure	Luminance/cd m^{-2}	Ref.
0D QDs	$CsPbBr_3$	479(≤ 20)	12.3	ITO/PEDOT:PSS/PTAA/Perovskite/TPBi/LiF/Al	90	[29]
	$CsPbBr_3$	470(27)	4.7	ITO/PEDOT:PSS/PVK /Perovskite/ZnO/Ag	3850	[81]
	$Rb_xCs_{1-x}PbBr_3$	490(24)	0.87	ITO/PEDOT:PSS/PolyTPD/Perovskite/TPBi/LiF/Al	186	[78]
	$CsPbCl_xBr_{3-x}$	455(20)	0.07	ITO/PEDOT:PSS/PVK /Perovskite/TPBi/LiF/Al	742	[9]
	$CsPb(Br/Cl)_3$	463(14)	1.4	ITO/PEDOT:PSS/Poly-TPD/CBP/Perovskite /B3PYMPM/ LiF/Al	318	[76]
	$CsMn_yPb_{1-y}Br_xCl_{3-x}$	466(17.9)	2.12	ITO/PEDOT:PSS/TFB/PFI/ Perovskite/ TPBi/LiF/Al	245	[53]
	$CsPbCl_xBr_{3-x}:Ni^{2+}$	470(NA)	2.4	ITO/PEDOT:PSS/TFB/PFI/ Perovskite/ TPBi/LiF/Al	612	[44]
	Cs_3Cu_2I5	445(~ 63)	1.12	ITO/p-NiO/Perovskite/ TPBi/LiF/Al	262.6	[79]
	$(Rb_{0.33}Cs_{0.67})_{0.42}FA_{0.58}PbCl_{1.25}Br_{1.75}$	466(23)	0.61	ITO /Poly-TPD/ Perovskite/ TPBi/Ba/Al	39	[77]
	$CsPb(Br_xCl_{1-x})_3$	471(17)	6.3	ITO/PEDOT:PSS/TFB /PFI /Perovskite /3TPYMB/Liq/Al	465	[43]
	$CsPb(Br/Cl)_3$	477(19)	1.96	ITO/PEDOT:PSS/Poly-TPD/PVK /Perovskite/PO-T2T/ LiF/Al	86.95	[42]
	$CsPb(Br/Cl)_3$	470(21)	2.15	ITO/PEDOT:PSS/Poly-TPD/PVK/Perovskite/TMPyPB / LiF/Al	507	[86]
	$CsPb(Br/Cl)_3$	463(17)	3.3	ITO/PEDOT:PSS/TFB /PFI /Perovskite /TPBi/LiF/Al	569	[85]
	$CsPbBr_{1.5}Cl_{1.5}$	480(17)	0.0074	ITO/ZnO/Perovskite/TFB/MoO_3/Ag	8.7	[87]
	$CsPbBr_xCl_{3-x}$	480(19)	0.86	ITO/PEDOT:PSS/Poly-TPD/Perovskite/TPBi/LiF/Al	29.95	[80]
	$CsPb(Br_{1-x}Cl_x)_3$	462/476/487(NA)	0.23/ 1.07/2.1	ITO/PEDOT:PSS/Poly-TPD/ PVK/Perovskite /B2PYMPM/ TPBi/LiF/Al	193/678/2063	[47]
	$CsPb(Cl/Br)_3$	456(15)	1.1	ITO/PEDOT:PSS/TFB /Perovskite /TPBi/Liq/Al	43.2	[49]
	$CsPbBr_xCl_{3-x}$	490(19)	1.9	ITO/PEDOT:PSS/PVK/ Perovskite /TPBi/LiF/Al	35	[46]
	$CsPb(Br_{1-x}Cl_x)_3$	495(21)	0.075	ITO/TiO_2/Perovskite/F8/MoO_3/Au	750	[48]
	$CsPbBr_xCl_{3-x}$	460(14.6)	1.35	ITO/PEDOT:PSS/Poly-TPD/Perovskite/TPBi/LiF/Al	33.0	[83]
	$CsPbBr_xCl_{3-x}$	469(24)	0.5	ITO/PEDOT:PSS/TFB /PFI/Perovskite /TPBi/LiF/Al	111	[75]
	$MAPbBr_xCl_{3-x}$	445(< 30)	1.38	ITO/PEDOT:PSS/PVK/ Perovskite /TPBi/LiF/Al	2673	[130]
	$CsPbBr_xCl_{3-x}$	470(~ 20)	0.07	ITO/NiO_X/Perovskite/ TPBi/LiF/Al	350	[40]
2D NPLs	$MAPbBr_3$	456(NA)	0.004	ITO/PEDOT:PSS/PVK/ Perovskite /TPBi/LiF/Al	~ 2	[61]
	$CsPbBr_3$	~ 480(NA)	~ 0.1	ITO/PEDOT:PSS/ Perovskite /TPBi/LiF/Ca/Al	25	[64]
	$CsPbBr_3$	464/489(16/26)	0.33/0.55	ITO/PEDOT:PSS/Poly-TPD(TFB)/ Perovskite /TPBi/LiF/Al	40/120	[88]
	$CsPbBr_3$	464 (18)	0.11	ITO/PEDOT:PSS/Poly-TPD/ Perovskite /TPBi/LiF/Al	29	[78]
	$CsPbBr_3$	464(< 20)	0.057	ITO/PEDOT:PSS/Poly-TPD/TAPC/ TPBi/Ca/Ag	38	[67]
	$(PEA)_2PbBr_4$	410(< 18)	0.31	ITO/PEDOT:PSS/PVK/TAPC/ TPBi/Ca/Ag	147.6	[90]

Notes: $EL_{\lambda max}$, peak value of electroluminescence spectra; EQE_{max}, maximum external quantum efficiency; FWHM, half peak width; NA, unknown content. The following table is also applicable.

emission layers of blue PeLEDs devices based 0D and 2D colloidal perovskites are spin-coated, which tallies with the target of solution-processed and large-area display technology. The optimization of luminescent LMHPs and charge transporting layers represent two main approaches for promoting device performance. The following parts will mainly revolve around device-level optimization based on 0D QDs and 2D NPLs. And the details of blue LEDs based on colloidal perovskites, including EL emission peak with FWHM, efficiency, luminance and device structure, are concluded in Table 1.

4.1. LEDs based on 0D QDs

As mentioned above, 0D QDs are also known as nanocrystals. During device fabrication, 0D QDs are usually deposited by directly spin-coating the nanocrystal solution (in toluene or cyclohexane) followed by a period of annealing, matching the demand of large-area interactive electronics with intelligent characteristics [3,70–74]. There is no doubt that high-performance LEDs are synergic action of multifunctional layers. Among them, charge transporting layers (CTLs) closely connected to active layers are essential components to achieve the optimum value. Elementary physical processes such as charge injection and light extraction are all extremely dependent on CTLs in LEDs. Recently, lots of outstanding works have been devoted to CTL-relative interface research in blue PeLEDs. N. Congreve et al. demonstrated that the emission efficiency and lifetime of prepared perovskite nanocrystals were significantly influenced by the selection of hole transporting layers [75]. When employed HTLs such as NiO_x, nonradiative recombination of the emissive state could be induced, further basically restricting device performance. And the alternate introduction of TFB/PFI maintained robust nanocrystal emission, achieving an external quantum efficiency (EQE) of 0.5% at 469 nm, which is seven times higher than that of control devices (Fig. 6c–e). Moreover, the deeper-lying valence band of 0D nanocrystals obstructs efficient hole injection. A stepwise injection strategy by employing two HTLs was implemented to solve this problem [76]. The stable electroluminescence peak wavelength of 463 nm and EQE of 1% were obtained. In addition to CTLs, the optimization of emissive QDs that determine the intrinsic luminescence performance is also crucial.

One of the most important reasons for low PLQY in the thin-film state is the non-radiative defects in perovskites with wider bandgap, and ion doping has been proved as a very effective method to benefit the active materials. For instance, carefully tuning of manganese (Mn) doping inside the Cl/Br-alloyed perovskite enables a three-fold increase of PLQY of nanocrystal films while maintaining pure blue electroluminescence without introducing Mn-emission peak [53] (Fig. 7a). Furthermore, enhanced photoluminescence lifetime and reduced trap states also demonstrated the practicality of doping. And developed doping devices presented a narrower electroluminescence peak and brighter blue color than undoped LEDs, allowing for an EQE of 2.12% at an emission peak of 466 nm (Fig. 7b, c). Constructing multiple A-site cations of perovskite nanocrystal is another way to breach the low-efficiency bottleneck of blue PeLEDs, which was more common in the perovskite solar cell community. Generally, out-of-center displacements of the octahedral framework would be tilted if accompanied by size changes of A-cite cations, further affecting the orbital overlap of halide anion and B-cite divalent cations. So wider tunability of perovskite nanocrystal bandgap can be obtained. Rubidium cation (Rb^+) was used to realize A-site doping for high-performance electroluminescent devices [77]. By multi-cation hot injecting, the initiator combining Rb^+ was reacted with FABr-modified precursor solution to produce deep-blue

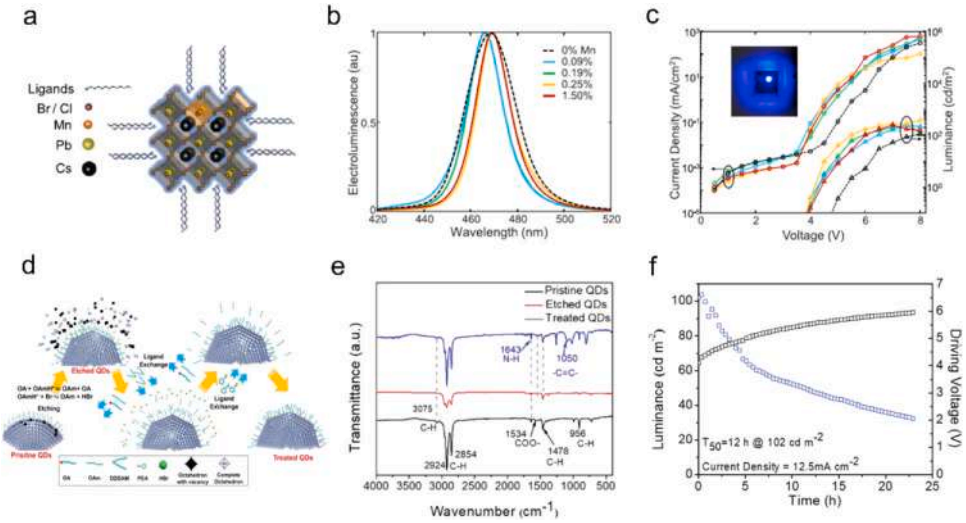

Fig. 7. (a) Diagram of Mn-doped nanocrystal structure. (b) Electroluminescence spectra and (c) *J-V-L* characteristic curve of constructed PeLEDs with different doping ratios of Mn^{2+}. Inset shows a picture of 0.19%-Mn^{2+}-doping device. Reprinted with permission [53]. Copyright 2018, Elsevier Science Inc. (d) Schematic picture of ligand exchange process driven by HBr etching. (e) FTIR results of pristine QDs, etched QDs and treated QDs (f) Operational half-lifetime (T_{50}) of the related blue LEDs at an initial brightness of 102 cd m^{-2}. Reprinted with permission [81]. Copyright 2021, Wiley-VCH.

$(Rb_{0.33}Cs_{0.67})_{0.42}FA_{0.58}PbCl_{1.25}Br_{1.75}$ QDs. Via octahedral distortions and quantum confinement effect caused by the small Rb^+, the blue shift of emission wavelength can be obtained. And the resultant perovskite QLEDs exhibited an EQE_{max} of 0.61% at 466 nm. Similarly, Rb^+ was also incorporated into $CsPbBr_3$ nanocrystals to yield stable blue emission through a mixed cation strategy [78]. Changes in Rb^+ content can tune emissions from 460 to 500 nm. When operating voltages reached 10 V, the newly-designed devices displayed color-pure stable EL, largely attributed to a pure bromine crystal structure. Peak EQE of 0.11% for 464 nm was obtained. This A-site doped strategy enabled good thermal and operational stability, providing a potential solution to overcome the shortcoming of halide segregation under external fields. Other ions such as Ni^+ were also used to dope $CsPbCl_xBr_{3-x}$ perovskite QDs for constructing bright blue LEDs [44], and a maximum luminance of 612 cd m^{-2}, EQE of 2.4% at 470 nm were obtained. Numerous alternative doping ions provide a huge space for the development of defect-lowered high-stable perovskite QLEDs. Moreover, most reported blue PeLEDs are lead-based. The toxicity of lead may cause serious environmental issues for practical commercialization. So, it is of great significance to gradually reduce or even completely eliminate dependence on lead. Shan et al. [79] demonstrated deep-blue LEDs based on ternary copper halide $Cs_3Cu_2I_5$ nanocrystals. The fabricated devices showed a EQE of 1.12% at 445 nm and a half-lifetime above 100 h, proving good operation stability of the eco-friendly element.

For perovskite QDs used to fabricate LEDs, photoluminescence and electroluminescence performance are usually not matched. Although equipped with exceptionally tunable optical characteristics and a high PLQY of more than 90%, the existence of relatively insulating long-chain ligands results in inefficient charge injection, which largely limits the improvement of EQE. Therefore, if the long-chain ligands are replaced with short-chain ligands based on ensuring the processing and stability of perovskite QDs, it will be of great benefit to the enhancement of device performance. Employing a short-chain halide ion pair, di-dodecyl dimethyl ammonium bromide (DDAB), to cap $CsPbX_3$ QDs for realizing stable films facilitates more efficient carrier transport [46]. The key to this ligand-exchange strategy lies in desorbing the protonated long-chain ligands. And a maximum EQE and luminance of 1.9% at 490 nm and 35 cd m^{-2} were achieved. DDAB and di-dodecyl dimethyl ammonium chloride (DDAC) was also used to reconstruct stable mixed-halide perovskite NCs via a ligand-mediated post-treatment method. Cl^- (Br^-) induced from DDAC (DDAB) can compensate for the Cl (Br) vacancy during the synthetic process of NCs. This self-anion exchange enables a max EQE of 0.86% and 0.44% at 480 ± 2 and 470 nm, respectively [80]. DDAB (DDAC) had been highly successful for a post-synthetic treatment during the formation of perovskite NCs. They were also used as a sole ligand system to directly synthesize uniform cuboid perovskite NCs [47]. As a result, the LED demonstrated high EQE values of 1.03% for EL peak position at 463 nm. Recently, Tian et al. [81] prepared stable small-sized $CsPbBr_3$ QDs (≈ 4 nm) by adopting a novel acid etching-driven ligand-exchange strategy with the aid of hydrochloric acid (HBr) etching. As schematically shown in Fig. 7d, the incomplete octahedrons were etched and excessive long-chain ligands were removed with the help of HBr. Then, the short-chain didodecylamine (DDDAM) and phenethylamine (PEA) were introduced to link with uncoordinated sites and exchange with residual long-chain oleic acid and oleylamine. According to Fourier-transform infrared spectroscopy (FTIR) results, the etched QDs exhibited weak C═O stretching and N−H bending vibration, and the ligands exchange process was confirmed by the presence of C═C stretching vibration from the benzene ring of PEA ligands (Fig. 7e). Compared with pristine QDs, the treated QDs equipped with short-chain DDDAM and PEA have much fewer vacancy defects, presenting a near-unity PLQY and good stability. The developed LEDs showed a robust durability at 470 nm with a half-life time of 12 h at initial luminance of 102 cd m^{-2} in operation, making a record life time of blue Pb-based perovskite LEDs (Fig. 7f). Ligand-exchange was also used in blue perovskite QLED with an emission wavelength below 470 nm. Kido et al. demonstrated that adamantine diamine (ADDA) with a rigid bidentate structure can be used for the improvement of PLQY and LED performance [49]. Assisted by a quaternary ammonium salt of interfacial layer, the fabricated blue LED exhibited a max EQE of 1.1% and luminance of 43.2 cd m^{-2} at 456 nm. And this method of replacing long-chain ligands with short-chain ligands has achieved great success. However, because of the intrinsic ionic nature of perovskite lattices, size changes induced by the regrowth of NCs during the replacing process make it difficult to ensure pre-designed emissive characteristics in LEDs. An alternative approach is to use conductive inorganic ligands [82]. The organic-ligand-lacking perovskite NCs applied for stable LEDs can be obtained by reasonably choosing halide-bearing ligands [83]. Based on a mild reaction of thionyl halides ($SOCl_2$, $SOBr_2$, or mixture thereof) with the amine and carboxylic groups on the surface of perovskite NCs, the produced

NCs showed good stability and high PLQY. Profiting from the fine-controlling severity of the reaction, excessive etching of uniformly sized NCs was avoided. And an attractive feature is the high film-forming property of synthesized NCs inks. The resultant blue perovskite NCs LEDs achieved a max EQE of 1.35% at 460 nm, with a FWHM of 14.6 nm. This solution-phase ligand-exchange strategy for preparing organic-ligand-lacking perovskite NCs provides a systematic solution for constructing efficient blue emissive devices with easier charge transport. Another issue of concern of ligand exchange is the destruction of the perovskite ionic structure by the existence of polar solvents. The terminating ion pairs on the surface of perovskite NCs and the organic ligands will be stripped off during the exchanging process, further destabilizing the colloid NCs. A bipolar-shell resurfacing strategy was pursued to construct strongly confined perovskite NCs [29]. The negatively charged inner shell and positively charged outer shell were adsorbed to each other by electrostatic force. Specifically, based on synthesized NCs, isopropylammonium bromide (IPABr) and NaBr were used to implement ligand exchange steps, respectively. The out shell of resurfaced perovskite NCs comprised of polar solvent molecules and the inner consisted of anion shell. The short inter-NC distance greatly promoted charge transport efficiency among resurfaced NCs when compared with traditional long-chain perovskite NCs. Motivated by the lowered trap density and improved mobility, the blue perovskite QLED based on resurfaced NCs demonstrated the highest EQE value of 12.3% at the EL position of 479 nm to date. Therefore, the suitable ligand management of perovskite NCs plays an important role in achieving efficient and stable perovskite LEDs. On the other hand, although surfactants are necessary to form stable colloidal MHP NCs in the traditional method, the dynamic equilibrium between unbound and bound ligands caused by proton exchange between acid and amine may enable ligands loss. Besides, OAm is also a reason for the degradation of NCs [84]. Synthesis of perovskite NCs through replacing amine for blue LEDs was proposed, such as tetraoctylammonium halides (TOAX) [48]. Despite a low EQE of 0.075% at 495 nm, this amine-free method without the post-anion exchange provides a solution for high-performance stable electroluminescent devices.

Passivation treatment to eliminate the trap defects is also vital for efficient PeLEDs. Employing a new type of short calcium–-tributylphosphine oxide (Ca–TBPO) complexes to passivate the surface of Cl-Br mixed MHP NCs for reducing non-radiative defects via halogen compensation, an EQE of 3.3% at 463 nm, which represented the highest value in the deep-blue range [85]. Similarly, the passivation of non-polar organic pseudohalide (n-dodecylammonium thiocyanate (DAT)) for Cl vacancies in mixed MHP NCs attributed in an EQE of 6.3% at 471 nm of fabricated blue LEDs [43]. And the passivation of phenethylammonium chloride to $CsPb(Cl/Br)_3$ perovskite NCs enabled an EQE of 0.77% at 462 nm and 2.15% at 470 nm [86]. As emission layers, perovskite NCs films are generally formed by spin-coating NCs solutions on charge transporting layers, and the subsequent deposition of CTLs may dissolve the NCs films. A trimethylaluminum (TMA) vapor-based crosslinking method was reported to chemically incorporate ligands into the alumina network which acted as a surface passivating agent, enhancing the thermal stability of emissive NCs [87]. In conclusion, through the optimization of device architecture and colloidal MHP NCs itself, blue LEDs will harvest strong performance improvement.

4.2. LEDs based on 2D NPLs

2D NPLs are also used to fabricate blue perovskite LEDs. However, uniformly distributed NPLs with tunable thickness and edge length are still unavailable owing to high growth rates. Many efforts have been devoted to overcoming these challenges. Ultrathin $CsPbBr_3$ NPLs with controllable dimensions were obtained by adjusting reaction kinetics without further purification steps [64]. The prototype of the blue LED prepared showed a maximum luminance of 25 cd m^{-2} and an EQE value of 0.1% at the EL position of 480 nm. Other works based on quantum-confined 2D NPLs also achieved decent device performances [64,88,89]. Assisted by poly (triarylamine) interlayers, the poor electronic interface between HTLs and emission layers could be optimized and interfacial non-radiative losses could be reduced. The EQE of 464 nm and EQE of 489 nm LED were 0.3% and 0.55%, respectively [88]. 2D Ruddlesden-Popper perovskite NPLs were another potential candidate for blue LEDs. Deng et al. demonstrated $(PEA)_2PbBr_4$-based (PEA = $C_8H_9NH_3$) blue LEDs at 410 nm [90]. The as-fabricated devices delivered a maximum luminance of 147.6 cd m^{-2} and an EQE_{max} of 0.31%. Furthermore, the EL intensity retained 80% after the 1350-min operational test, proving the great potential of 2D perovskite for the development of stable blue LEDs.

5. Quasi-2D perovskites for blue PeLEDs

5.1. Optical properties of quasi-2D perovskites

As mentioned above, 2D colloidal NPLs possess strong exciton binding energy when the number of perovskite octahedral layers is no more than 4 [91,92]. As shown in Fig. 8a, quasi-2D perovskites are a combination of 2D perovskites with small-n values ($n \leq 4$) and 3D perovskites or 2D perovskites with large-n values [93,94]. In other words, quasi-2D perovskites possess not only few layer 2D NPLs with sufficient excitons but also 3D perovskites with deficient excitons [95–97]. Typically, quasi-2D perovskites have a prevailing formula of $L_2(APbX_3)_{n-1}PbX_4$ (Ruddlesden–Popper phase) or $L(APbX_3)_{n-1}PbX_4$ (Dion–Jacobson phase), where L is an organic spacer cation (such as butylammonium (BA), phenylethylammonium (PEA), and 1,4-diaminobutane (DAB)), A stands for monovalent cations (Cs^+, MA^+, FA^+, etc.), X is halide and n represents the number of stacking perovskite units. When the organic cations in the A-site is large enough that the bulk perovskite structure cannot be maintained, the perovskite lattice will be separated along with the < 100 > crystal orientation to partially form a two-dimensional layered structure. On one hand, Ruddlesden–Popper (RP) phase containing two spacer monocations is formed by cutting along the < 100 > plane in bulk perovskites, exhibiting a staggered configuration. On the other hand, Dion–Jacobson (DJ) phase containing diamine spacer cations is derived from bulk perovskites with no shift between the two adjacent layered perovskites using the same approach as the RP phase. (Fig. 8b) [98]. Especially, the concentration of organic cations in precursor solution plays an important role in determining the thickness of inorganic layers, and phase distribution could be affected by various organic cations. In recent years, numerous investigations on quasi-2D perovskites for high-performance photoelectric devices have been reported by many groups due to their outstanding photoelectric conversion efficiency, good moisture stability [99,100], confined charge carrier balance, and state-of-the-art pinhole-free film as the LED emitters [101,102]. The bandgap of quasi-2D perovskites can be tuned by modulating the number of perovskite octahedron layers (n) (Fig. 8c). Intriguingly, the photoluminescence (PL) spectrum of quasi-2D perovskites appears as multiple luminescence peaks but the electroluminescence (EL) spectrum is a single luminescence peak. Herein, charge transfer or energy transfer in multi-quantum wells may unravel the above phenomenon [93,103,104]. The charge recombination occurs in a high-n quantum well eventually via charge transfer or energy transfer driven by electric field. Therefore, only a single peak can be observed in the EL spectra. Originally, Huang's group [93] prepared a $NFPbI_4$ film to demonstrate that energy transfer from quantum wells with large exciton energies ($n \leq 4$) to quantum wells with lower exciton energies. As a result, the electron-hole recombination process is completed in a narrow

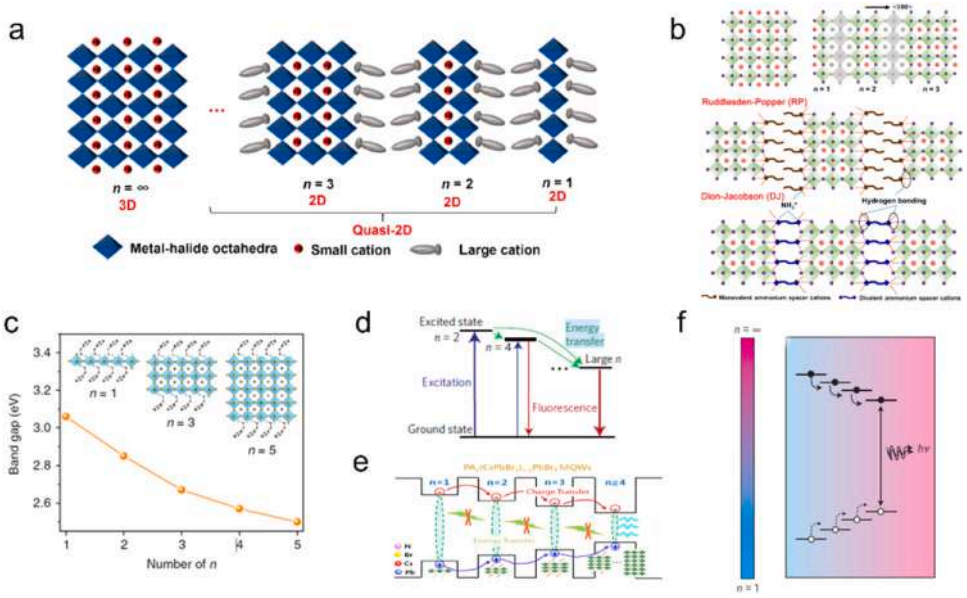

Fig. 8. Schematics of the properties of quasi-2D perovskites. (a) Schematic illustration of quasi-2D perovskites. Reprinted with permission [94]. Copyright 2020, American Chemical Society. (b) RP phase with monoamine cations and DJ phase with diamine monoamine in < 100 > crystal direction. Reprinted with permission [98]. Copyright 2019, American Chemical Society. (c) Tuning the bandgap by varying the number of stacking regular octahedral. Reprinted with permission [111]. Copyright 2016, Springer Nature. (d) Schematic illustration of energy transfer. Reprinted with permission [93]. Copyright 2016, Springer Nature. (e) Schematic of charge transfer in multiple quantum wells. Reprinted with permission [104]. Copyright 2018, Elsevier Science Inc. (f) Schematic diagram of carrier transfer in $PA_2(CsPbBr_3)_{n-1}PbBr_4$ quasi-2D perovskite. Reprinted with permission [103]. Copyright 2016, Springer Nature.

bandgap quantum well with high-n thickness (Fig. 8d). Chen et al. [104] investigated the charge transfer in $PA_2(CsPbBr_3)_{n-1}PbBr_4$ quantum wells. They hold the view that charge transfer is more significant than energy transfer because quasi-2D perovskite quantum wells have a high dielectric constant (ε) which is inversely proportional to the rate of energy transfer (Fig. 8e). In addition, apart from charge transferring in inherent quantum wells, the process was also found among adjacent grains by Sargent's group [103]. The results of transient absorption (TA) and time-resolved PL spectroscopy indicated that the downward funneling of energy was complete from higher energy states to lower energy states, and residual dynamic recombination would occur in the lowest-energy inclusions after around 100 ps (Fig. 8f). On the other hand, there are several drawbacks to quasi-2D perovskites. Because of inefficient energy transfer, quasi-2D perovskites always contain multiple phase structures and undesirable impurity phase, which lead to low external quantum efficiency [101,105]. Meanwhile, they suffer from poor spectral stability as a result of unavoidable van der Waals gaps caused by the spacer monoammonium organic cations [106].

5.2. LEDs based on quasi-2D perovskites

Initially, quasi-2D perovskite was applied in solar cells to address the water-oxygen stability issues caused by the chemical decomposition of regular 3D perovskites in a humid environment [99,107]. Lee's group [108] firstly took a hack at employing quasi-2D perovskites as emitters in visible green PeLEDs, eventually producing an optimum device with a current efficiency of 4.90 cd A^{-1} and maximum luminance (2935 cd m^{-2}) at 520 nm. Many researchers have investigated blue-emitting PeLEDs using quasi-2D perovskites in recent years, owing to their high exciton binding energy and good environmental stability [105,109–111]. In contrast to colloidal perovskite QDs/NPLs, quasi-2D perovskite thin films are formed using solution-based in-situ growth rather than synthesized colloidal nanocrystals. Therefore, the proper large organic cations are vital for perovskite films with high crystalline quality, even device performance. The conventional organic cations in quasi-2D perovskites have been widely used in LEDs, like arylamines and alkylamines [94]. In 2016, Cheng and co-workers [22] reported the first sky-blue PeLEDs based on 4-$PBA_2(CsPbBr_3)_{n-1}PbBr_4$ perovskites, showing an EQE of 0.015% at a brightness of 186 cd m^{-2}. Despite the low efficiency of devices, this report proves that quasi-2D perovskite has real potential for blue LED application in the future. Yip's group [112] further explored 2-phenoxyethylamine (POEA) as an organic spacer into $CH_3NH_3PbBr_3$ precursor solution. As illustrated in Fig. 9a, with increasing concentration of POEA, both the color emission of PL and EL spectrum shifted from green to blue. Finally, a 60%-POEA device showed an emission peak at 462 nm, delivering a brightness of 19.5 cd A^{-1} and an EQE of 1.1%. Likewise, Vashishtha et al. [113] produced perovskite RP phase using butylammonium as a separating ligand. The as-obtained blue PeLED showed an EQE of 2.4% and 6.2% at a wavelength of 465 nm and 487 nm, respectively. Li et al. [109] firstly demonstrated sky-blue LEDs based on $PEA_2Cs_{n-1}Pb_n(Cl_xBr_{1-x})_{3n+1}$. The introduction of PEA^+ into the precursor solution not only reduced the trap states but also strikingly improved the PLQYs of films from 0.15% to a maximum of 27%. Also, they controlled the thickness of hole transporting layers (HTL) to modulate the recombination zone on top of perovskite layers, suggesting the thinner (≈ 30 nm) HTL controlled, the better performance devices obtained (Fig. 9b). Finally, a maximum luminance of 3780 cd m^{-2} and the best EQE of 5.7% at 480 nm was achieved (Fig. 9c). In quasi-2D perovskite LEDs, PEA is a widely used organic ligand due to its high triplet energy level which enables generating electron-hole pairs to improve radiative recombination [114]. However, this large bulky organic ligand with strong van der Waals interaction is favorable to facilitating the formation of 2D perovskites (n under a current density 1), which is harmful to exciton energy transfer [111]. It is reported that the notorious 2D phase (n = 1) leads to nonradiative recombination but the popular phases with other small-n values such as n = 2, 3, and 4 are beneficial to energy transfer and more efficient blue emitting [115]. In 2018, Xing et al. [111] replaced partially long ligands (PEABr) by short ligands, iso-propylammonium bromide (IPABr). Blue shift is evidently shown in film PL spectra, suggesting IBABr additive can promote the formation of small n

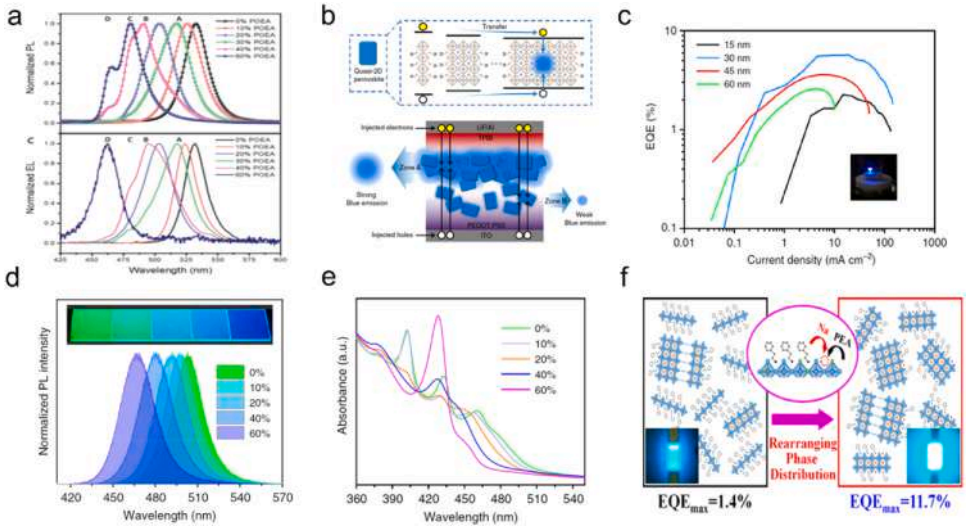

Fig. 9. (a) PL spectra of $MAPbBr_3$ precursor with different contents of POEA and EL spectra of corresponding perovskite LEDs. Reprinted with permission [112]. Copyright 2017, Wiley-VCH. (b) The top diagram showed that energy transfer or charge transfer occurs in a quasi-2D structure after charge injection. The bottom diagram illustrated the distribution of perovskite crystals in luminescent layer, where a strong blue emitting can be observed in Zone A and the Zone B shows a weak blue emission after electrons and holes recombining by carrier injection. And (c) EQE diagram of 100%-PEA $PEA_2Cs_{n-1}Pb_n(Cl_xBr_{1-x})_{3n+1}$ perovskite LEDs with different PEDOT: PSS thickness and photo of the device while operating. Reprinted with permission [109]. Copyright 2019, Springer Nature. (d) PL and (e) absorption spectra of quasi-2D $PEA_2(MA/Cs)_{1.5}Pb_{2.5}Br_{8.5}$ with 0–60% isopropylammonium bromide (IPA) additive. Insets are UV-irradiation films with different IPA contents. Reprinted with permission [111]. Copyright 2018, Springer Nature. (f) Schematic diagram showing the rearrangement of phase distribution by Na^+ additive, and the related device insets based on quasi-2D perovskites. Reprinted with permission [115]. Copyright 2020, American Chemical Society.

phase (Fig. 9d). Meanwhile, as the concentration of IPABr added increased, the blue shift of absorption edge was observed in Fig. 9e, attributing to growth of intermediate n phase and the suppression of lowest-n and highest-n phases (n = 2, 3, 4). $PEA_2A_{n-1}Pb_nX_{3n+1}$ perovskite film displayed color-stable blue emission (477 nm) with a PLQY of 88% by mixed ligands engineering. The resulting sky-blue LEDs exhibited a maximum luminance of 2480 cd m^{-2} and an EQE_{max} of 1.5% at the EL emission of 490 nm. This proves that the introduction of mixed ligands into perovskite precursors is an effective way of enabling the narrowed phase distribution, and improving the film's stability and PLQYs. Similarly, Jin et al. [116] utilized the synergistic effect of dual ligands, PEABr and $NPABr_2$ (N-(2-Bromoethyl)-1,3-propanediamine dihydrobromide), to fabricate spectrally stable PeLEDs under continuously operating conditions. The final LED showed a maximum EQE of 2.62% and a half lifetime (T_{50}) of 8.8 min. Other ligands mixing with PEABr not only enhance the PLQYs of the film and the external quantum efficiency of devices, but also stabilize photoluminescence spectra of film and electroluminescence spectra of blue PeLEDs, such as 1,4-Bis(aminomethyl) benzene bromide (P-$PDABr_2$) [117], ethylenediammonium dibromide ($EDABr_2$) [118], i-butylammonium bromide (iBABr) [110], diphenylphosphinic chloride (DPPOCl) [119] and so on. In addition to organic ligands, inorganic salts can also control the growth of quantum wells. Huang's group [120] obtained wide-bandgap perovskites by incorporating PEACl (phenylethylammonium chloride) and YCl_3 (Yttrium(III) chloride) into $CsPbBr_3$ perovskite films to enhance the PLQY from 1.1% to 49.7%. After the introduction of YCl_3, the charge carriers were confined inside perovskite grains for more radiative recombination. Inspiringly, with the aid of PEACl and YCl_3 ligands, the corresponding devices have a high EQE value, reaching 4.8% at 477 nm and 11.0% at 485 nm. Pang et al. [115] rearranged the phase distribution by incorporating NaBr solution. As shown in Fig. 9f, the incorporation of the sodium ions with PEA can reduce the formation of the n = 1 phase and increase the proportion of other small-n phases. After treatment, the relative sky-blue LED, with a high EQE of 11.7% and a stable emission peak at 488 nm, was achieved.

Furthermore, other strategies for improving the efficiency and stability of quasi-2D PeLEDs have been explored, containing doping [105,121], dimensional engineering [122], and modifying the hole transporting layer [123,124]. It is known that the perovskite layer is susceptible to ion migration and phase separation, making the EL spectrum unstable. A-site doping in quasi-2D perovskite is a plausible strategy to realize blue emission with an unchanged spectrum. In 2019, Jiang et al. [105] fabricated spectrally stable blue PeLEDs based on Rb-doping quasi-2D perovskite, < n > = 3 $PEA_2(Rb_xCs_{1-x})_2Pb_3Br_{10}$. By adding an excess amount of RbBr, the PLQY of film soared up to 82%. Accordingly, the corresponding LEDs displayed blue-emission at 475 nm with a half-life time of 14.5 min, and the EL peak emission remained the same at continuous driving voltages (Fig. 10a). Chu et al. [121] further explored the A-site doping by adding the large cation $CH_3CH_2NH_2^+$ (EA^+) (Fig. 10b). Based on sky-blue PeLEDs with 60% EABr, they demonstrated that the emission spectra are stable under applied voltage, delivering a luminescence of 2191 cd m^{-2} and 12.1% EQE at a peak EL of 488 nm under a current density of 17.58 cd A^{-1}, (Fig. 10c). Mass undesirable nonradiative recombination at the interface, between transporting layer and perovskite film, is responsible for lagging blue PeLEDs. Choy's group [123] applied hole transporting bilayer structure composed of PSSNa and NiO_x to inhibit the nonradiative decays by reducing the defects in NiO_x and improving the morphology of perovskite film. They further incorporated KBr into the quasi-2D perovskite for amending the quality of perovskite film. Consequently, the carrier injection barrier was reduced resulting from the band gap shift of transporting and perovskite layers (Fig. 10d). Taking this idea into consideration, Shen et al. [124] used a K^+-modified hole transporting layers (HTL) to passivate the halide defects at the HTL/perovskite interface and guide the growth of quasi-2D perovskite, thereby indirectly enabling a more unhindered hole transporting (Fig. 10e). In the end, the high-efficiency deep-blue LED with a maximum EQE of 4.14% at EL of 469 nm was realized (Fig. 10f). Moreover, an ultrathin emissive layer, comprising quantum-confined nanoparticles embedded in quasi-2D phases, was prepared by Liu et al. [122]. The blue-emission perovskite film with higher bandgaps was composed of major quasi-2D perovskites with some QDs. Based on this quantum-fined blue film, they further adopted the antisolvent strategy with the aim of dissolving excess organic ligands (phenylbutylammonium bromide, PBABr), which effectively reduce the charge-injection barriers causing by PBABr. Finally, with a high EQE of 9.5% at 483 nm, the

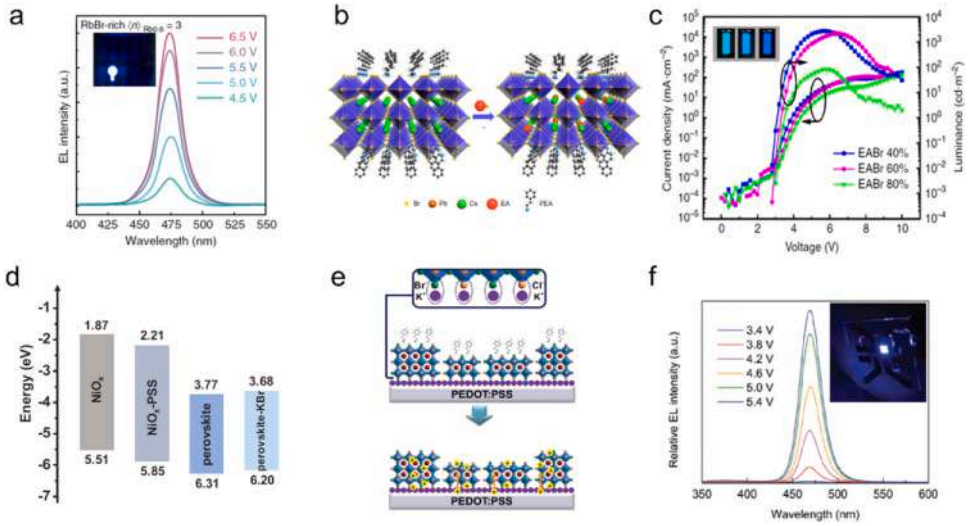

Fig. 10. (a) Stable EL spectra of the Rb-doping $PEA_2(Rb_xCs_{1-x})_2Pb_3Br_{10}$ LED and inset image shows the electroluminescence of the related LED. Reprinted with permission [105]. Copyright 2019, Springer Nature. (b) Schematics depicting $CH_3CH_2NH_2^+$ (EA^+) cation doping into the host lattice to partially replace Cs^+. (c) Schematics characterizing the current density and luminance of EABr-doped quasi-2D PeLEDs. Inset shows the electroluminescence photos of PeLEDs with 40%, 60% and 80% EABr. Reprinted with permission [121]. Copyright 2020, Springer Nature. (d) Schematic picture showing energy level of PSSNa-treated NiO_x and K^+-treated perovskite layer. Reprinted with permission [123]. Copyright 2020, Wiley-VCH. (e) Schematic diagram of growth of quasi-2D perovskites guided by K^+-modified HTL. (f) EL spectra under continuous increasing bias voltages based on K^+-modified PeLED and inset is an electroluminescent image. Reprinted with permission [124]. Copyright 2020, Wiley-VCH.

color-pure blue LED was fabricated. Lately, Ren et al. [106] thought that the weak van der Waals gaps could cause perovskite phase scattering with a loose connection, which might lead to inefficient energy transfer. It also deteriorated the stability of the perovskite structure with easy degradation during LED operating. They introduced 4-(2-aminoethyl) benzoic acid (ABA) into perovskite to diminish this bad effect for promoting coupled quasi-2D perovskite layers. Finally, the improved devices showed a high peak EQE of 10.11% and long-time operational stability of 81.3 min. Until now, Wang et al. [125] achieved one of the best pure-blue quasi-2D LEDs by the incorporation of a chelating additive molecule, γ-aminobutyric acid (GABA). They thought GABA could suppress the growth of thicker quantum wells (n > 3) by coordinating the $PbBr_2$ molecules. The treated film appeared bluer spectra in contrast with original film, with the reason that electron-hole recombination process was finished in a low-n quantum well (n = 3). A true-blue LED at 478 nm was thus demonstrated using a device structure of ITO/PEDOT: PSS/PVK: PFI/$PEA_2Cs_{n-1}Pb_nBr_{3n+1}$/TPBi/LiF/Al, presenting an EQE of 6.3% and a luminance of 17 cd m^{-2} (Fig. 11). So far, the details of blue PeLEDs based on quasi-2D perovskites are also summarized in Table 2.

Although quasi-2D perovskites have been successfully utilized in fabricating high-performance blue LEDs, most of the EL spectra at 480–490 nm, which are not suitable for the blue range according to National Television System Committee (NTSC) standard. And the EL spectra based on blue PeLEDs is supposed to be located in a bluer region. Therefore, the relative research on perovskite LEDs in bluer ranges should attract more attention in terms of promoting device performance.

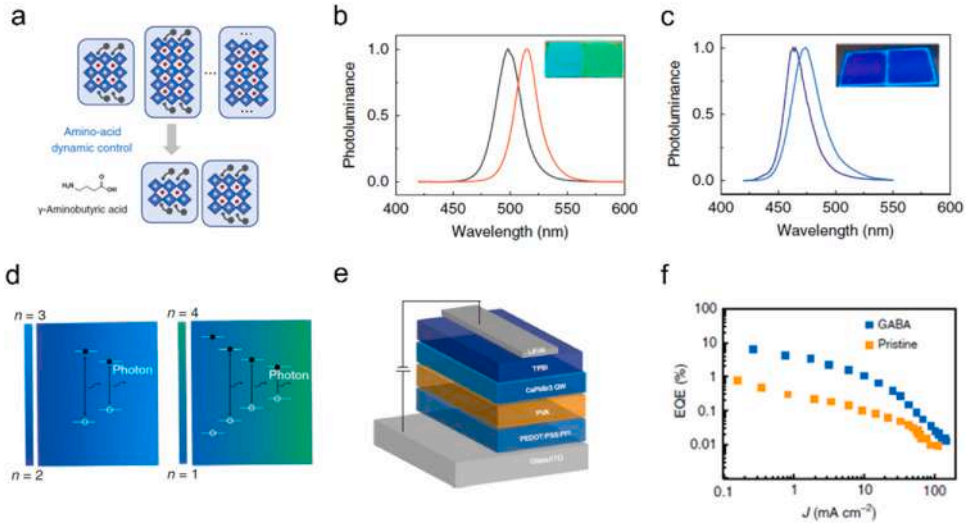

Fig. 11. Characterization of pure-blue LED based on GABA-treated quasi-2D perovskite film with its properties. (a) Schematic showing the inhibition of high-n quantum wells by GABA. (b) PL spectra of pristine film and (c) GABA-treated film. Inset are green and blue photoluminescence under UV photoexcitation in respective diagrams. (d) Electron-hole recombination process in GABA-treated device and control device. (e) Schematic drawing of device structure. (f) Schematic diagram of EQE for the control group. Reprinted with permission [125]. Copyright 2020, Wiley-VCH.

Table 2
Recent progress of blue PeLEDs based on quasi-2D perovskites.

	Perovskites	$EL_{\lambda max}$ (FWHM)/nm	EQE_{max}/%	Device structure	Luminance/cd m^{-2}	Ref.
Quasi-2D perovskites	$(PEOA)_2(MA)_{n-1}Pb_nBr_{3n+1}$	494(NA)	1.1	ITO/PEDOT:PSS/Perovskite/TPBI/Ba/Al	19.25	[112]
	$IPA/PEA_2MA/Cs_{n-1}Pb_nBr_{3n-1}$	490(28)	1.5	ITO/PEDOT:PSS/Perovskite/TPBi/LiF/Al	2480	[111]
	$BA_2Cs_{n-1}Pb_n(Br/Cl)_{3n+1}$	465(NA)	2.4	ITO/PEDOT:PSS/PVK/Perovskite/TPBi/Al	962	[113]
	$PEA_2Cs_{n-1}Pb_n(Cl_xBr_{1-x})_{3n+\ 1}$	480(21)	5.7	ITO/PEDOT:PSS/Perovskite/TPBi/LiF/Al	3780	[109]
	YCl_3/PEACl:$CsPbBr_3$	485(NA)	11	ITO/PEDOT:PSS/Perovskite/TPBI/LiF/Al	9040	[120]
	$PA_2(CsPbBr_3)_{n-1}PbBr_4$	492(~ 26)	1.45	ITO/NiO_x/PSSNa/Perovskite/TPBi/LiF/Al	4359	[123]
	$PEA_2(Rb_xCs_{1-x})_2Pb_3Br_{10}$	475(20)	1.35	ITO/PEDOT:PSS/Perovskite/TmPyPB/LiF/Al	100.6	[105]
	P-PDA/$PEACs_{n-1}Pb_nBr_{3n+1}$	465(25)	2.6	ITO/PVK/PFI/Perovskite/3TPYMB/Liq/Al	211	[117]
	$PEA_2NPA_1Cs_2Pb_3Br_{12}$	485(~ 23)	2.62	ITO/PVK/Perovskite/PO-T2T/Liq/Al	1200	[116]
	$PEABr:FA_{0.3}Cs_{0.7}PbBr_3$	483(26)	9.5	ITO/NiO_x/TFB/PVK/Perovskite/TPBi/LiF/Al	54	[122]
	$DPPOCl:PEA_2Cs_{1.6}MA_{0.4}Pb_3Br_{10}$	479(18)	5.2	ITO/PEDOT:PSS:PFI/Perovskite/TPBi/LiF/Al	468	[119]
	$[(PEA)_{0.75}(GA)_{0.25}]_2CsPb_2X_7$	492(17.8)	8.2	ITO/PVK:F4-TCNQ/Perovskite/TPPO/TPBi/LiF/Al	1003	[131]
	$(BA_XPEA_{1-X})_2Cs_{n-1}Pb_n(Br_{0.7}Cl_{0.3})_{3n+1}$	485(NA)	7.84	ITO/PEDOT:PSS/Perovskite/TPBi/Ca/Al	1130	[110]
	GABA-$PEA_2Cs_{n-1}Pb_nBr_{3n+1}$	478(NA)	6.3	ITO/PEDOT:PSS/PVK:PFI/Perovskite/TPBI/LiF/Al	200	[125]
	NaBr:PEA-$CsPb(Br_xCl_{1-x})_3$	488(18.8)	11.7	ITO/NiOx/PTAA/PVK/Perovskite/TPBi/LiF/Al	1511	[115]
	$PEA_2(Cs_{1-x}EA_xPbBr_3)_2PbBr_4$	488(25)	12.1	ITO/m-PEDOT:PSS/Perovskite/TBPi /LiF /Al	2191	[121]
	$EDA_2[PEAPbBr_3]_{n-1}PbBr_4$	474(26)	2.17	ITO/PEDOT:PSS/Perovskite/TPBi/LiF/Al	290	[118]
	$FAPbBr_{3-x}Cl_x$	473(NA)	3.1	ITO/PEDOT:PSS/Perovskite/B3PYMPM/LiF/Al	2810	[132]
	F-PEABr:$CsPbBr_{1.5}Cl_{1.5}$	469(21)	4.14	ITO/PEDOT:PSS/Perovskite/TPBi/LiF/Al	451	[124]
	ABA-$PEA_XPA_{2-X}(CsPbBr_3)_{n-1}PbBr_4$	486(25)	10.11	ITO/PVK/Perovskite/TPBi/LiF/Al	513	[106]

6. Summary and outlook

6.1. Improving device stability and efficiency

In comparison with green/red PeLEDs, there are still plenty of room for improvement of blue-emissive PeLEDs. Although blue-emitting LMHPs have achieved a high PLQY reaching 100% in the colloidal solution state, the widely recognized concerns about PeLEDs such as poor stability, low efficiency, and slight luminance still remain a baffling challenge to this date. The reasons for lagging development of blue PeLEDs can be drawn to as-prepared materials, film formation and device fabrication. Firstly, the as-prepared nanocrystals have abundant inherent defects which easily form trap states, weakening the optical properties. A soft ionic crystal structure capped with highly dynamic organic ligands is responsible for the instability of blue-emitting nanocrystals. For example, bromide-based blue perovskites (QDs or NPLs) easily tend to agglomerate, and mixed-halide perovskites severely suffer from phase segregation. Second, it is incapable to precisely control perovskite growth kinetics during film formation, leading to generation of undesired impurity phase. Many organic ligands of colloidal nanocrystals will be lost during spin-coating process, causing the serious degradation of the optical properties of perovskite film. Finally, because of a deep valence band (≈ 6.1 eV) [75] in blue-emitting perovskites, large hole-injection barrier, and emission quenching between CTLs and perovskites are not favorable to electro-optical conversion efficiency.

In the case of colloidal perovskite NCs (0D) or NPLs (2D), we need to find more reasonable methods for minimizing surface defect density for high PLQY and optimizing organic ligands for better charge injection of the device. Doping impurity ions into the perovskite host (ABX_3) is quite beneficial in meliorating optical properties. Specifically, A-site dopants such as Rb^+, FA^+, MA^+, K^+ could stabilize crystal structures and thereby the spectrally stable emission can be observed. B-site doping can easily tune the luminescence properties and suppress some inherent defects, such as Mn^{2+} , Al^{3+}, Cd^{2+}, Sn^{2+}, Cu^{2+} and so on. The surface capping ligands can stabilize nanoparticles in blue-emissive LMHPs, but they also greatly hinder carrier injection efficiency while the LED is running. Ligand exchanging for the surface chemical environment modulation of LMHPs by replacing traditionally organic long-chain OAm/OA is an effective approach to facilitate carrier transport and injection efficiency, e.g., DDAB, ADDA, IPABr and so on. In a nutshell, the trade-off between charge injection efficiency and stability of blue wide-bandgap LMHPs should be clarified for high-performance blue LEDs.

Phase segregation in mixed halide perovskites, whether colloidal nanocrystals or quasi-2D perovskites, is a long-lasting severe issue that brings about spectrally unstable and short operating time [126]. Driven by electric current, the blue-emissive $CsPb(Cl_xBr_{1-x})_3$ perovskites segregate into Cl-rich phase and Br-rich phase, causing the EL spectrum shift towards the green domain [87]. Since the weak-defect-tolerance $CsPbCl_3$ phase is responsible for instability of mixed halide perovskites, defect passivation for $CsPbCl_3$ phase is quite necessary. Significantly, the Cl defects can be generally repaired in two approaches: one is to passivate Cl vacancy by introducing Lewis base (e.g., quaternary ammonium bromide, pyridine) or inorganic halide salts (e.g., $NiCl_2$, YCl_3); the other one is to fasten Cl^- to avoid the ions migration by using functional ligands. For example, Ma et al. [119] demonstrated a novel chloride insertion-immobilization strategy by using diphenylphosphinyl chloride (DPPOCl) to restrain phase segregation and thereby developed a stable sky-blue LED with an excellent operational lifetime (T_{50} = 90 min, at initial luminance of 100 cd m^{-2}). Besides, the experience of solving phase separation in perovskite solar cells can be used for reference, such as the vapor-assistance-crystallization method [127,128]. More importantly, the mechanism of phase separation should be taken into consideration in great depth.

The elaborative design of device architecture should also be considered as well. And alternative CTLs should be utilized to match blue deep-energy-bandgap perovskite well. Additionally, the interface charge loss between CTL and perovskite layer should be reduced by regulating the transporting layer. Interfacial defect passivation and hole-electron injection balance should be also carefully explored. Moreover, the interfacial physical mechanism ought to be deeply understood under device operating conditions.

6.2. Developing deep-blue PeLEDs

Generally, the blue emissive range can be divided into three light emitting regions, involving sky-blue (490–475 nm), pure-blue (475–465 nm), and deep-blue (420–465 nm) [59]. Following NTSC

(Rec. 2020), the chromaticity coordinate of blue light is (0.131, 0.046), which means blue LED is supposed to emit at around 465 nm or bluer. Nevertheless, the deep-blue PeLEDs still run into some obstacles in both efficiency and stability due to higher carrier injection barriers and greater halide vacancy defects compared with sky-blue PeLEDs. The most baffling barrier in developing advanced deep-blue PeLEDs lies in devising high-efficient materials and matching the energy levels between perovskite layer and CTLs.

For colloidal nanocrystals (QDs or NPLs), there are several approaches to realizing deep-blue luminescent perovskite. One method is to increase more Cl contents into mixed halide nanocrystals to enlarge the bandgap. Obviously, chlorine vacancy originated from uncoordinated Cl ions in perovskites can introduce deep defect levels as the carrier traps, resulting in nonradiative recombination [50,129]. Thus, the deep-blue mixed halide nanocrystals with many defects should be passivated by short-chain capping ligands (e.g., thionyl halides ($SOCl_2$/$SOBr_2$)) or inorganic salts (e.g., YCl_3, $PrCl_3$). Preparing wider-bandgap perovskite via strong quantum-confined synthesis of ultra-small nanocrystals or B-site doping represents another approach, such as Cu-doping [79]. As for quasi-2D perovskite, thickness control of perovskite layer for charge transfer confinement can achieve bluer-emitting LEDs, which is conducive to the recombination of electron-hole in small-n quantum wells (n = 2, 3). However, these low-n phases can only be generated by introducing more organic ligands, and thermal exciton quenching could easily occur in small-n quantum wells [59], resulting in inefficient charge injection at the interface between CTLs and quasi-2D perovskite emitting layers. Therefore, controlling the growth kinetics by small organic molecules (e.g., γ-aminobutyric acid [125]) could be a promising strategy for achieving high-efficiency deep-blue LEDs.

In conclusion, with simultaneously considering the optimization of low-dimensional metal halide perovskites and relative LED architecture, we believe that high-efficiency and high-stability deep-blue LEDs will be realized for extensive optoelectronic applications.

Declaration of Competing Interest

The authors declare that they have no known competing financial interests or personal relationships that could have appeared to influence the work reported in this paper.

Acknowledgments

X.P. and C.Y. contributed equally to this work. This work is financially supported by Young Scientific and Technological Innovation Research Team Funds of Sichuan Province (Nos. 20CXTD0106 and 2019YFG0292), and Fundamental Research Funds for the Central Universities (No. 2682020CX06).

References

[1] X.K. Liu, W. Xu, S. Bai, Y. Jin, J. Wang, R.H. Friend, F. Gao, Metal halide perovskites for light-emitting diodes, Nat. Mater. 20 (2021) 10–21.
[2] P. Zhu, J. Zhu, Low-dimensional metal halide perovskites and related optoelectronic applications, InfoMat 2 (2020) 341–378.
[3] S. Chu, W. Chen, Z. Fang, X. Xiao, Y. Liu, J. Chen, J. Huang, Z. Xiao, Large-area and efficient perovskite light-emitting diodes via low-temperature blade-coating, Nat. Commun. 12 (2021) 147.
[4] Z. Fang, W. Chen, Y. Shi, J. Zhao, S. Chu, J. Zhang, Z. Xiao, Dual passivation of perovskite defects for light-emitting diodes with external quantum efficiency exceeding 20%, Adv. Funct. Mater. 30 (2020) 1909754.
[5] S. Xu, A. Libanori, G. Luo, J. Chen, Engineering bandgap of $CsPbI_3$ over 1.7 ev with enhanced stability and transport properties, iScience 24 (2021) 102235.
[6] M. Xie, H. Liu, F. Chun, W. Deng, C. Luo, Z. Zhu, M. Yang, Y. Li, W. Li, W. Yan, W. Yang, Aqueous phase exfoliating quasi-2D $CsPbBr_3$ nanosheets with ultrahigh intrinsic water stability, Small 15 (2019) 1901994.
[7] D. Meggiolaro, S.G. Motti, E. Mosconi, A.J. Barker, J. Ball, C. Andrea Riccardo Perini, F. Deschler, A. Petrozza, F. De Angelis, Iodine chemistry determines the defect tolerance of lead-halide perovskites, Energy Environ. Sci. 11 (2018) 702–713.
[8] F. Chun, B. Zhang, Y. Li, W. Li, M. Xie, X. Peng, C. Yan, Z. Chen, H. Zhang, W. Yang, Internally-externally defects-tailored $MAPbI_3$ perovskites with highly enhanced air stability and quantum yield, Chem. Eng. J. 399 (2020) 125715.
[9] J. Song, J. Li, X. Li, L. Xu, Y. Dong, H. Zeng, Quantum dot light-emitting diodes based on Inorganic perovskite cesium lead halides ($CsPbX_3$), Adv. Mater. 27 (2015) 7162–7167.
[10] M.V. Kovalenko, L. Protesescu, M.I. Bodnarchuk, Properties and potential optoelectronic applications of lead halide perovskite nanocrystals, Science 358 (2017) 745–750.
[11] L.M. Herz, Charge-carrier dynamics in organic-inorganic metal halide perovskites, Annu. Rev. Phys. Chem. 67 (2016) 65–89.
[12] M.E. Kamminga, H.-H. Fang, M.R. Filip, F. Giustino, J. Baas, G.R. Blake, M.A. Loi, T.T.M. Palstra, Confinement effects in low-dimensional lead iodide perovskite hybrids, Chem. Mater. 28 (2016) 4554–4562.
[13] P. Gao, A.R. Bin Mohd Yusoff, M.K. Nazeeruddin, Dimensionality engineering of hybrid halide perovskite light absorbers, Nat. Commun. 9 (2018) 5028.
[14] Z. Yang, M. Wang, H. Qiu, X. Yao, X. Lao, S. Xu, Z. Lin, L. Sun, J. Shao, Engineering the exciton dissociation in quantum-confined 2D $CsPbBr_3$ nanosheet films, Adv. Funct. Mater. 28 (2018) 1705908.
[15] Y. Fu, H. Zhu, J. Chen, M.P. Hautzinger, X.Y. Zhu, S. Jin, Metal halide perovskite nanostructures for optoelectronic applications and the study of physical properties, Nat. Rev. Mater. 4 (2019) 169–188.
[16] K. Hong, Q.V. Le, S.Y. Kim, H.W. Jang, Low-dimensional halide perovskites: review and issues, J. Mater. Chem. C 6 (2018) 2189–2209.
[17] Y.-H. Kim, S. Kim, A. Kakekhani, J. Park, J. Park, Y.-H. Lee, H. Xu, S. Nagane, R.B. Wexler, D.-H. Kim, S.H. Jo, L. Martínez-Sarti, P. Tan, A. Sadhanala, G.-S. Park, Y.-W. Kim, B. Hu, H.J. Bolink, S. Yoo, R.H. Friend, A.M. Rappe, T.-W. Lee, Comprehensive defect suppression in perovskite nanocrystals for high-efficiency light-emitting diodes, Nat. Photonics 15 (2021) 148–155.
[18] T. Chiba, Y. Hayashi, H. Ebe, K. Hoshi, J. Sato, S. Sato, Y.-J. Pu, S. Ohisa, J. Kido, Anion-exchange red perovskite quantum dots with ammonium iodine salts for highly efficient light-emitting devices, Nat. Photonics 12 (2018) 681–687.
[19] W. Xu, Q. Hu, S. Bai, C. Bao, Y. Miao, Z. Yuan, T. Borzda, A.J. Barker, E. Tyukalova, Z. Hu, M. Kawecki, H. Wang, Z. Yan, X. Liu, X. Shi, K. Uvdal, M. Fahlman, W. Zhang, M. Duchamp, J.-M. Liu, A. Petrozza, J. Wang, L.-M. Liu, W. Huang, F. Gao, Rational molecular passivation for high-performance perovskite light-emitting diodes, Nat. Photonics 13 (2019) 418–424.
[20] S. Peng, S. Wang, D. Zhao, X. Li, C. Liang, J. Xia, T. Zhang, G. Xing, Z. Tang, Pure bromide-based perovskite nanoplatelets for blue light-emitting diodes, Small Methods 3 (2019) 1900196.
[21] N.K. Kumawat, A. Dey, A. Kumar, S.P. Gopinathan, K.L. Narasimhan, D. Kabra, Band gap tuning of $CH_3NH_3Pb(Br_{1-x}Cl_x)_3$ hybrid perovskite for blue electroluminescence, ACS Appl. Mater. Interfaces 7 (2015) 13119–13124.
[22] L. Cheng, Y. Cao, R. Ge, Y.-Q. Wei, N.-N. Wang, J.-P. Wang, W. Huang, Sky-blue perovskite light-emitting diodes based on quasi-two-dimensional layered perovskites, Chin. Chem. Lett. 28 (2017) 29–31.
[23] Y.H. Kim, C. Wolf, Y.T. Kim, H. Cho, W. Kwon, S. Do, A. Sadhanala, C.G. Park, S.W. Rhee, S.H. Im, R.H. Friend, T.W. Lee, Highly efficient light-emitting diodes of colloidal metal-halide perovskite nanocrystals beyond quantum size, ACS Nano 11 (2017) 6586–6593.
[24] V.K. Ravi, A. Swarnkar, R. Chakraborty, A. Nag, Excellent green but less impressive blue luminescence from $CsPbBr_3$ perovskite nanocubes and nanoplatelets, Nanotechnology 27 (2016) 325708.
[25] H. Shao, X. Bai, G. Pan, H. Cui, J. Zhu, Y. Zhai, J. Liu, B. Dong, L. Xu, H. Song, Highly efficient and stable blue-emitting $CsPbBr_3$@SiO_2 nanospheres through low temperature synthesis for nanoprinting and WLED, Nanotechnology 29 (2018) 285706.
[26] S. Wang, C. Bi, J. Yuan, L. Zhang, J. Tian, Original core-shell structure of cubic $CsPbBr_3$@amorphous $CsPbBr_x$ perovskite quantum dots with a high blue photoluminescence quantum yield of over 80%, ACS Energy Lett. 3 (2017) 245–251.
[27] J. Li, L. Gan, Z. Fang, H. He, Z. Ye, Bright tail states in blue-emitting ultrasmall perovskite quantum dots, J. Phys. Chem. Lett. 8 (2017) 6002–6008.
[28] Y. Dong, T. Qiao, D. Kim, D. Parobek, D. Rossi, D.H. Son, Precise control of quantum confinement in cesium lead halide perovskite quantum dots via thermodynamic equilibrium, Nano Lett. 18 (2018) 3716–3722.
[29] Y. Dong, Y.K. Wang, F. Yuan, A. Johnston, Y. Liu, D. Ma, M.J. Choi, B. Chen, M. Chekini, S.W. Baek, L.K. Sagar, J. Fan, Y. Hou, M. Wu, S. Lee, B. Sun, S. Hoogland, R. Quintero-Bermudez, H. Ebe, P. Todorovic, F. Dinic, P. Li, H.T. Kung, M.I. Saidaminov, E. Kumacheva, E. Spiecker, L.S. Liao, O. Voznyy, Z.H. Lu, E.H. Sargent, Bipolar-shell resurfacing for blue LEDs based on strongly confined perovskite quantum dots, Nat. Nanotechnol. 15 (2020) 668–674.
[30] S. Seth, T. Ahmed, A. De, A. Samanta, Tackling the defects, stability, and photoluminescence of $CsPbX_3$ perovskite nanocrystals, ACS Energy Lett. 4 (2019) 1610–1618.
[31] C.H. Lu, G.V. Biesold-McGee, Y. Liu, Z. Kang, Z. Lin, Doping and ion substitution in colloidal metal halide perovskite nanocrystals, Chem. Soc. Rev. 49 (2020) 4953–5007.
[32] L. Protesescu, S. Yakunin, S. Kumar, J. Bar, F. Bertolotti, N. Masciocchi, A. Guagliardi, M. Grotevent, I. Shorubalko, M.I. Bodnarchuk, C.J. Shih, M.V. Kovalenko, Dismantling the "Red Wall" of colloidal perovskites: highly luminescent formamidinium and formamidinium-cesium lead iodide nanocrystals, ACS Nano 11 (2017) 3119–3134.
[33] M. Imran, J. Ramade, F. Di Stasio, M. De Franco, J. Buha, S. Van Aert, L. Goldoni, S. Lauciello, M. Prato, I. Infante, S. Bals, L. Manna, Alloy $CsCd_xPb_{1-x}Br_3$ perovskite nanocrystals: the role of surface passivation in preserving composition and blue emission, Chem. Mater. 32 (2020) 10641–10652.

[34] W. van der Stam, J.J. Geuchies, T. Altantzis, K.H. van den Bos, J.D. Meeldijk, S. Van Aert, S. Bals, D. Vanmaekelbergh, C. de Mello Donega, Highly emissive divalent-ion-doped colloidal $CsPb_{1-x}M_xBr_3$ perovskite nanocrystals through cation exchange, J. Am. Chem. Soc. 139 (2017) 4087–4097.

[35] L. Xu, S. Yuan, H. Zeng, J. Song, A comprehensive review of doping in perovskite nanocrystals/quantum dots: evolution of structure, electronics, optics, and light-emitting diodes, Mater. Today Nano 6 (2019) 100036.

[36] M. Liu, G.H. Zhong, Y.M. Yin, J.S. Miao, K. Li, C.Q. Wang, X.R. Xu, C. Shen, H. Meng, Aluminum-doped cesium lead bromide perovskite nanocrystals with stable blue photoluminescence used for display backlight, Adv. Sci. 4 (2017) 1700335(Weinh.).

[37] M. Leng, Y. Yang, Z. Chen, W. Gao, J. Zhang, G. Niu, D. Li, H. Song, J. Zhang, S. Jin, J. Tang, Surface passivation of bismuth-based perovskite variant quantum dots to achieve efficient blue emission, Nano Lett. 18 (2018) 6076–6083.

[38] M. Leng, Y. Yang, K. Zeng, Z. Chen, Z. Tan, S. Li, J. Li, B. Xu, D. Li, M.P. Hautzinger, Y. Fu, T. Zhai, L. Xu, G. Niu, S. Jin, J. Tang, All-inorganic bismuth-based perovskite quantum dots with bright blue photoluminescence and excellent stability, Adv. Funct. Mater. 28 (2018) 1704446.

[39] Z. Tan, J. Li, C. Zhang, Z. Li, Q. Hu, Z. Xiao, T. Kamiya, H. Hosono, G. Niu, E. Lifshitz, Y. Cheng, J. Tang, Highly efficient blue-emitting Bi-doped Cs_2SnCl_6 perovskite variant: photoluminescence induced by impurity doping, Adv. Funct. Mater. 28 (2018) 1801131.

[40] E.P. Yao, Z. Yang, L. Meng, P. Sun, S. Dong, Y. Yang, Y. Yang, High-brightness blue and white leds based on inorganic perovskite nanocrystals and their composites, Adv. Mater. 29 (2017) 1606859.

[41] L. Protesescu, S. Yakunin, M.I. Bodnarchuk, F. Krieg, R. Caputo, C.H. Hendon, R.X. Yang, A. Walsh, M.V. Kovalenko, Nanocrystals of cesium lead halide perovskites ($CsPbX_3$, X = Cl, Br, and I): novel optoelectronic materials showing bright emission with wide color gamut, Nano Lett. 15 (2015) 3692–3696.

[42] F. Yang, H. Chen, R. Zhang, X. Liu, W. Zhang, J. Zhang, F. Gao, L. Wang, Efficient and spectrally stable blue perovskite light-emitting diodes based on potassium passivated nanocrystals, Adv. Funct. Mater. 30 (2020) 1908760.

[43] X. Zheng, S. Yuan, J. Liu, J. Yin, F. Yuan, W.-S. Shen, K. Yao, M. Wei, C. Zhou, K. Song, B.-B. Zhang, Y. Lin, M.N. Hedhili, N. Wehbe, Y. Han, H.-T. Sun, Z.-H. Lu, T.D. Anthopoulos, O.F. Mohammed, E.H. Sargent, L.-S. Liao, O.M. Bakr, Chlorine vacancy passivation in mixed halide perovskite quantum dots by organic pseudohalides enables efficient Rec. 2020 blue light-emitting diodes, ACS Energy Lett. 5 (2020) 793–798.

[44] G. Pan, X. Bai, W. Xu, X. Chen, Y. Zhai, J. Zhu, H. Shao, N. Ding, L. Xu, B. Dong, Y. Mao, H. Song, Bright blue light emission of Ni^{2+} ion-doped $CsPbCl_xBr_{3-x}$ perovskite quantum dots enabling efficient light-emitting devices, ACS Appl. Mater. Interfaces 12 (2020) 14195–14202.

[45] J. De Roo, M. Ibanez, P. Geiregat, G. Nedelcu, W. Walravens, J. Maes, J.C. Martins, I. Van Driessche, M.V. Kovalenko, Z. Hens, Highly dynamic ligand binding and light absorption coefficient of cesium lead bromide perovskite nanocrystals, ACS Nano 10 (2016) 2071–2081.

[46] J. Pan, L.N. Quan, Y. Zhao, W. Peng, B. Murali, S.P. Sarmah, M. Yuan, L. Sinatra, N.M. Alyami, J. Liu, E. Yassitepe, Z. Yang, O. Voznyy, R. Comin, M.N. Hedhili, O.F. Mohammed, Z.H. Lu, D.H. Kim, E.H. Sargent, O.M. Bakr, Highly efficient perovskite-quantum-dot light-emitting diodes by surface engineering, Adv. Mater. 28 (2016) 8718–8725.

[47] Y. Shynkarenko, M.I. Bodnarchuk, C. Bernasconi, Y. Berezovska, V. Verteletskyi, S.T. Ochsenbein, M.V. Kovalenko, Direct synthesis of quaternary alkylammonium-capped perovskite nanocrystals for efficient blue and green light-emitting diodes, ACS Energy Lett. 4 (2019) 2703–2711.

[48] E. Yassitepe, Z. Yang, O. Voznyy, Y. Kim, G. Walters, J.A. Castañeda, P. Kanjanaboos, M. Yuan, X. Gong, F. Fan, J. Pan, S. Hoogland, R. Comin, O.M. Bakr, L.A. Padilha, A.F. Nogueira, E.H. Sargent, Amine-free synthesis of cesium lead halide perovskite quantum dots for efficient light-emitting diodes, Adv. Funct. Mater. 26 (2016) 8757–8763.

[49] T. Chiba, S. Ishikawa, J. Sato, Y. Takahashi, H. Ebe, S. Ohisa, J. Kido, Blue perovskite nanocrystal light-emitting devices via the ligand exchange with adamantane diamine, Adv. Opt. Mater. 8 (2020) 2000289.

[50] G.H. Ahmed, J.K. El-Demellawi, J. Yin, J. Pan, D.B. Velusamy, M.N. Hedhili, E. Alarousu, O.M. Bakr, H.N. Alshareef, O.F. Mohammed, Giant photoluminescence enhancement in $CsPbCl_3$ perovskite nanocrystals by simultaneous dual-surface passivation, ACS Energy Lett. 3 (2018) 2301–2307.

[51] C. Luo, W. Li, D. Xiong, J. Fu, W. Yang, Surface pre-optimization of a mixed halide perovskite toward high photoluminescence quantum yield in the blue spectrum range, Nanoscale 11 (2019) 15206–15215.

[52] C. Bi, S. Wang, Q. Li, S.V. Kershaw, J. Tian, A.L. Rogach, Thermally stable copper (II)-doped cesium lead halide perovskite quantum dots with strong blue emission, J. Phys. Chem. Lett. 10 (2019) 943–952.

[53] S. Hou, M.K. Gangishetty, Q. Quan, D.N. Congreve, Efficient blue and white perovskite light-emitting diodes via manganese doping, Joule 2 (2018) 2421–2433.

[54] J. Tang, K.W. Kemp, S. Hoogland, K.S. Jeong, H. Liu, L. Levina, M. Furukawa, X. Wang, R. Debnath, D. Cha, K.W. Chou, A. Fischer, A. Amassian, J.B. Asbury, E.H. Sargent, Colloidal-quantum-dot photovoltaics using atomic-ligand passivation, Nat. Mater. 10 (2011) 765–771.

[55] B.T. Diroll, G. Nedelcu, M.V. Kovalenko, R.D. Schaller, High-temperature photoluminescence of $CsPbX_3$ (X = Cl, Br, I) nanocrystals, Adv. Funct. Mater. 27 (2017) 1606750.

[56] A. Dualeh, P. Gao, S.I. Seok, M.K. Nazeeruddin, M. Grätzel, Thermal behavior of methylammonium lead-trihalide perovskite photovoltaic light harvesters, Chem. Mater. 26 (2014) 6160–6164.

[57] C. Luo, C. Yan, W. Li, F. Chun, M. Xie, Z. Zhu, Y. Gao, B. Guo, W. Yang, Ultrafast thermodynamic control for stable and efficient mixed halide perovskite nanocrystals, Adv. Funct. Mater. 30 (2020) 2000026.

[58] P. Tyagi, S.M. Arveson, W.A. Tisdale, Colloidal organohalide perovskite nanoplatelets exhibiting quantum confinement, J. Phys. Chem. Lett. 6 (2015) 1911–1916.

[59] G. Zou, Z. Chen, Z. Li, H.-L. Yip, Blue perovskite light-emitting diodes: opportunities and challenges, Acta Phys. Chim. Sin. 0 (2020) 2009002-2009000.

[60] J.A. Sichert, Y. Tong, N. Mutz, M. Vollmer, S. Fischer, K.Z. Milowska, R. Garcia Cortadella, B. Nickel, C. Cardenas-Daw, J.K. Stolarczyk, A.S. Urban, J. Feldmann, Quantum size effect in organometal halide perovskite nanoplatelets, Nano Lett. 15 (2015) 6521–6527.

[61] S. Kumar, J. Jagielski, S. Yakunin, P. Rice, Y.C. Chiu, M. Wang, G. Nedelcu, Y. Kim, S. Lin, E.J.G. Santos, M.V. Kovalenko, C.J. Shih, Efficient blue electroluminescence using quantum-confined two-dimensional perovskites, ACS Nano 10 (2016) 9720–9729.

[62] M.C. Weidman, M. Seitz, S.D. Stranks, W.A. Tisdale, Highly tunable colloidal perovskite nanoplatelets through variable cation, metal, and halide composition, ACS Nano 10 (2016) 7830–7839.

[63] J. Huang, Y.-H. Wu, Z.-G. Zhu, W.Y. Shih, W.-H. Shih, Control of oleylamine to perovskite ratio in synthesis of $MAPbBr_3$ nanoparticles, Chem. Phys. Lett. 702 (2018) 21–25.

[64] D. Yang, Y. Zou, P. Li, Q. Liu, L. Wu, H. Hu, Y. Xu, B. Sun, Q. Zhang, S.-T. Lee, Large-scale synthesis of ultrathin cesium lead bromide perovskite nanoplates with precisely tunable dimensions and their application in blue light-emitting diodes, Nano Energy 47 (2018) 235–242.

[65] Y. Bekenstein, B.A. Koscher, S.W. Eaton, P. Yang, A.P. Alivisatos, Highly luminescent colloidal nanoplates of perovskite cesium lead halide and their oriented assemblies, J. Am. Chem. Soc. 137 (2015) 16008–16011.

[66] Z. Liang, S. Zhao, Z. Xu, B. Qiao, P. Song, D. Gao, X. Xu, Shape-controlled synthesis of all-inorganic $CsPbBr_3$ perovskite nanocrystals with bright blue emission, ACS Appl. Mater. Interfaces 8 (2016) 28824–28830.

[67] B.J. Bohn, Y. Tong, M. Gramlich, M.L. Lai, M. Doblinger, K. Wang, R.L.Z. Hoye, P. Muller-Buschbaum, S.D. Stranks, A.S. Urban, L. Polavarapu, J. Feldmann, Boosting tunable blue luminescence of halide perovskite nanoplatelets through postsynthetic surface trap repair, Nano Lett. 18 (2018) 5231–5238.

[68] Y. Wu, C. Wei, X. Li, Y. Li, S. Qiu, W. Shen, B. Cai, Z. Sun, D. Yang, Z. Deng, H. Zeng, In situ passivation of $PbBr_6^{4-}$ octahedra toward blue luminescent $CsPbBr_3$ nanoplatelets with near 100% absolute quantum yield, ACS Energy Lett. 3 (2018) 2030–2037.

[69] J. Shamsi, D. Kubicki, M. Anaya, Y. Liu, K. Ji, K. Frohna, C.P. Grey, R.H. Friend, S.D. Stranks, Stable hexylphosphonate-capped blue-emitting quantum-confined $CsPbBr_3$ nanoplatelets, ACS Energy Lett. 5 (2020) 1900–1907.

[70] N. Zhang, J. Chen, Y. Huang, W. Guo, J. Yang, J. Du, X. Fan, C. Tao, A wearable all-solid photovoltaic textile, Adv. Mater. 28 (2016) 263–269.

[71] G. Chen, Y. Li, M. Bick, J. Chen, Smart textiles for electricity generation, Chem. Rev. 120 (2020) 3668–3720.

[72] N. Zhang, F. Huang, S. Zhao, X. Lv, Y. Zhou, S. Xiang, S. Xu, Y. Li, G. Chen, C. Tao, Y. Nie, J. Chen, X. Fan, Photo-rechargeable fabrics as sustainable and robust power sources for wearable bioelectronics, Matter 2 (2020) 1260–1269.

[73] J. Chen, Y. Huang, N. Zhang, H. Zou, R. Liu, C. Tao, X. Fan, Z.L. Wang, Micro-cable structured textile for simultaneously harvesting solar and mechanical energy, Nat. Energy 1 (2016) 16138.

[74] X. Chu, X. Zhao, Y. Zhou, Y. Wang, X. Han, Y. Zhou, J. Ma, Z. Wang, H. Huang, Z. Xu, C. Yan, H. Zhang, W. Yang, J. Chen, An ultrathin robust polymer membrane for wearable solid-state electrochemical energy storage, Nano Energy 76 (2020) 105179.

[75] M.K. Gangishetty, S. Hou, Q. Quan, D.N. Congreve, Reducing architecture limitations for efficient blue perovskite light-emitting diodes, Adv. Mater. 30 (2018) 1706226.

[76] S.T. Ochsenbein, F. Krieg, Y. Shynkarenko, G. Raino, M.V. Kovalenko, Engineering color-stable blue light-emitting diodes with lead halide perovskite nanocrystals, ACS Appl. Mater. Interfaces 11 (2019) 21655–21660.

[77] F. Meng, X. Liu, X. Cai, Z. Gong, B. Li, W. Xie, M. Li, D. Chen, H.L. Yip, S.J. Su, Incorporation of rubidium cations into blue perovskite quantum dot light-emitting diodes via FABr-modified multi-cation hot-injection method, Nanoscale 11 (2019) 1295–1303.

[78] P. Todorović, D. Ma, B. Chen, R. Quintero-Bermudez, M.I. Saidaminov, Y. Dong, Z.H. Lu, E.H. Sargent, Spectrally tunable and stable electroluminescence enabled by rubidium doping of $CsPbBr_3$ nanocrystals, Adv. Opt. Mater. 7 (2019) 1901440.

[79] L. Wang, Z. Shi, Z. Ma, D. Yang, F. Zhang, X. Ji, M. Wang, X. Chen, G. Na, S. Chen, D. Wu, Y. Zhang, X. Li, L. Zhang, C. Shan, Colloidal synthesis of ternary copper halide nanocrystals for high-efficiency deep-blue light-emitting diodes with a half-lifetime above 100h, Nano Lett. 20 (2020) 3568–3576.

[80] Y.S. Shin, Y.J. Yoon, K.T. Lee, J. Jeong, S.Y. Park, G.H. Kim, J.Y. Kim, Vivid and fully saturated blue light-emitting diodes based on ligand-modified halide perovskite nanocrystals, ACS Appl. Mater. Interfaces 11 (2019) 23401–23409.

[81] C. Bi, Z. Yao, X. Sun, X. Wei, J. Wang, J. Tian, Perovskite quantum dots with ultralow trap density by acid etching-driven ligand exchange for high luminance and stable pure-blue light-emitting diodes, Adv. Mater. 33 (2021) 2006722, https://doi.org/10.1002/adma.202006722

[82] X. Li, Y.-B. Zhao, F. Fan, L. Levina, M. Liu, R. Quintero-Bermudez, X. Gong, L.N. Quan, J. Fan, Z. Yang, S. Hoogland, O. Voznyy, Z.-H. Lu, E.H. Sargent, Bright colloidal quantum dot light-emitting diodes enabled by efficient chlorination, Nat. Photonics 12 (2018) 159–164.

[83] B.B. Zhang, S. Yuan, J.P. Ma, Y. Zhou, J. Hou, X. Chen, W. Zheng, H. Shen, X.C. Wang, B. Sun, O.M. Bakr, L.S. Liao, H.T. Sun, General mild reaction creates highly luminescent organic-ligand-lacking halide perovskite nanocrystals for efficient light-emitting diodes, J. Am. Chem. Soc. 141 (2019) 15423–15432.

[84] N.C. Anderson, M.P. Hendricks, J.J. Choi, J.S. Owen, Ligand exchange and the stoichiometry of metal chalcogenide nanocrystals: spectroscopic observation of facile metal-carboxylate displacement and binding, J. Am. Chem. Soc. 135 (2013) 18536–18548.

[85] J. Yao, L. Wang, K. Wang, Y. Yin, J. Yang, Q. Zhang, H. Yao, Calcium-tributylphosphine oxide passivation enables the efficiency of pure-blue perovskite light-emitting diode up to 3.3%, Sci. Bull. 65 (2020) 1150–1153.

[86] H. Shao, Y. Zhai, X. Wu, W. Xu, L. Xu, B. Dong, X. Bai, H. Cui, H. Song, High brightness blue light-emitting diodes based on $CsPb(Cl/Br)_3$ perovskite QDs with phenethylammonium chloride passivation, Nanoscale 12 (2020) 11728–11734.

[87] G. Li, F.W. Rivarola, N.J. Davis, S. Bai, T.C. Jellicoe, F. de la Pena, S. Hou, C. Ducati, F. Gao, R.H. Friend, N.C. Greenham, Z.K. Tan, Highly efficient perovskite nanocrystal light-emitting diodes enabled by a universal crosslinking method, Adv. Mater. 28 (2016) 3528–3534.

[88] R.L.Z. Hoye, M.L. Lai, M. Anaya, Y. Tong, K. Galkowski, T. Doherty, W. Li, T.N. Huq, S. Mackowski, L. Polavarapu, J. Feldmann, J.L. MacManus-Driscoll, R.H. Friend, A.S. Urban, S.D. Stranks, Identifying and reducing interfacial losses to enhance color-pure electroluminescence in blue-emitting perovskite nanoplatelet light-emitting diodes, ACS Energy Lett. 4 (2019) 1181–1188.

[89] D.N. Congreve, M.C. Weidman, M. Seitz, W. Paritmongkol, N.S. Dahod, W.A. Tisdale, Tunable light-emitting diodes utilizing quantum-confined layered perovskite emitters, ACS Photonics 4 (2017) 476–481.

[90] W. Deng, X. Jin, Y. Lv, X. Zhang, X. Zhang, J. Jie, 2D Ruddlesden-popper perovskite nanoplate based deep-blue light-emitting diodes for light communication, Adv. Funct. Mater. 29 (2019) 1903861.

[91] T. Ishihara, J. Takahashi, T. Goto, Exciton state in two-dimensional perovskite semiconductor $(C_{10}H_{21}NH_3)_2PbI_4$, Solid State Commun. 69 (1989) 933–936.

[92] D.B. Straus, C.R. Kagan, Electrons, excitons, and phonons in two-dimensional hybrid perovskites: connecting structural, optical, and electronic properties, J. Phys. Chem. Lett. 9 (2018) 1434–1447.

[93] N. Wang, L. Cheng, R. Ge, S. Zhang, Y. Miao, W. Zou, C. Yi, Y. Sun, Y. Cao, R. Yang, Y. Wei, Q. Guo, Y. Ke, M. Yu, Y. Jin, Y. Liu, Q. Ding, D. Di, L. Yang, G. Xing, H. Tian, C. Jin, F. Gao, R.H. Friend, J. Wang, W. Huang, Perovskite light-emitting diodes based on solution-processed self-organized multiple quantum wells, Nat. Photonics 10 (2016) 699–704.

[94] L. Zhu, D. Liu, J. Wang, N. Wang, Large organic cations in quasi-2D perovskites for high-performance light-emitting diodes, J. Phys. Chem. Lett. 11 (2020) 8502–8510.

[95] D. Liang, Y. Peng, Y. Fu, M.J. Shearer, J. Zhang, J. Zhai, Y. Zhang, R.J. Hamers, T.L. Andrew, S. Jin, Color-pure violet-light-emitting diodes based on layered lead halide perovskite nanoplates, ACS Nano 10 (2016) 6897–6904.

[96] B.R. Sutherland, E.H. Sargent, Perovskite photonic sources, Nat. Photonics 10 (2016) 295–302.

[97] K. Tanaka, T. Takahashi, T. Kondo, K. Umeda, K. Ema, T. Umebayashi, K. Asai, K. Uchida, N. Miura, Electronic and excitonic structures of inorganic–organic perovskite-type quantum-well crystal $(C_4H_9NH_3)_2PbBr_4$, Jpn. J. Appl. Phys. 44 (2005) 5923–5932.

[98] P. Huang, S. Kazim, M. Wang, S. Ahmad, Toward phase stability: Dion-Jacobson layered perovskite for solar cells, ACS Energy Lett. 4 (2019) 2960–2974.

[99] I.C. Smith, E.T. Hoke, D. Solis-Ibarra, M.D. McGehee, H.I. Karunadasa, A layered hybrid perovskite solar-cell absorber with enhanced moisture stability, Angew. Chem. Int. Ed. 53 (2014) 11232–11235.

[100] H. Tsai, W. Nie, J.-C. Blancon, C.C. Stoumpos, R. Asadpour, B. Harutyunyan, A.J. Neukirch, R. Verduzco, J.J. Crochet, S. Tretiak, L. Pedesseau, J. Even, M.A. Alam, G. Gupta, J. Lou, P.M. Ajayan, M.J. Bedzyk, M.G. Kanatzidis, A.D. Mohite, High-efficiency two-dimensional Ruddlesden–Popper perovskite solar cells, Nature 536 (2016) 312–316.

[101] X. Yang, X. Zhang, J. Deng, Z. Chu, Q. Jiang, J. Meng, P. Wang, L. Zhang, Z. Yin, J. You, Efficient green light-emitting diodes based on quasi-two-dimensional composition and phase engineered perovskite with surface passivation, Nat. Commun. 9 (2018) 570.

[102] J. Qing, X.-K. Liu, M. Li, F. Liu, Z. Yuan, E. Tiukalova, Z. Yan, M. Duchamp, S. Chen, Y. Wang, S. Bai, J.-M. Liu, H.J. Snaith, C.-S. Lee, T.C. Sum, F. Gao, Aligned and graded Type-II Ruddlesden-Popper perovskite films for efficient solar cells, Adv. Energy Mater. 8 (2018) 1800185.

[103] M. Yuan, L.N. Quan, R. Comin, G. Walters, R. Sabatini, O. Voznyy, S. Hoogland, Y. Zhao, E.M. Beauregard, P. Kanjanaboos, Z. Lu, D.H. Kim, E.H. Sargent, Perovskite energy funnels for efficient light-emitting diodes, Nat. Nanotechnol. 11 (2016) 872–877.

[104] P. Chen, Y. Meng, M. Ahmadi, Q. Peng, C. Gao, L. Xu, M. Shao, Z. Xiong, B. Hu, Charge-transfer versus energy-transfer in quasi-2D perovskite light-emitting diodes, Nano Energy 50 (2018) 615–622.

[105] Y. Jiang, C. Qin, M. Cui, T. He, K. Liu, Y. Huang, M. Luo, L. Zhang, H. Xu, S. Li, J. Wei, Z. Liu, H. Wang, G.H. Kim, M. Yuan, J. Chen, Spectra stable blue perovskite light-emitting diodes, Nat. Commun. 10 (2019) 1868.

[106] Z. Ren, J. Yu, Z. Qin, J. Wang, J. Sun, C.C.S. Chan, S. Ding, K. Wang, R. Chen, K.S. Wong, X. Lu, W.J. Yin, W.C.H. Choy, High-performance blue perovskite light-emitting diodes enabled by efficient energy transfer between coupled quasi-2D perovskite layers, Adv. Mater. 33 (2020) 2005570.

[107] Z. Song, A. Abate, S.C. Watthage, G.K. Liyanage, A.B. Phillips, U. Steiner, M. Graetzel, M.J. Heben, Improving the photovoltaic performance of perovskite solar cells with acetate, Sci. Rep. 6 (2016) 38670.

[108] J. Byun, H. Cho, C. Wolf, M. Jang, A. Sadhanala, R.H. Friend, H. Yang, T.W. Lee, Efficient visible quasi-2D perovskite light-emitting diodes, Adv. Mater. 28 (2016) 7515–7520.

[109] Z. Li, Z. Chen, Y. Yang, Q. Xue, H.L. Yip, Y. Cao, Modulation of recombination zone position for quasi-two-dimensional blue perovskite light-emitting diodes with efficiency exceeding 5, Nat. Commun. 10 (2019) 1027.

[110] F. Wang, Z. Wang, W. Sun, Z. Wang, Y. Bai, T. Hayat, A. Alsaedi, Z. Tan, High performance quasi-2D perovskite sky-blue light-emitting diodes using a dual-ligand strategy, Small 16 (2020) 2002940.

[111] J. Xing, Y. Zhao, M. Askerka, L.N. Quan, X. Gong, W. Zhao, J. Zhao, H. Tan, G. Long, L. Gao, Z. Yang, O. Voznyy, J. Tang, Z.H. Lu, Q. Xiong, E.H. Sargent, Color-stable highly luminescent sky-blue perovskite light-emitting diodes, Nat. Commun. 9 (2018) 3541.

[112] Z. Chen, C. Zhang, X.F. Jiang, M. Liu, R. Xia, T. Shi, D. Chen, Q. Xue, Y.J. Zhao, S. Su, H.L. Yip, Y. Cao, High-performance color-tunable perovskite light emitting devices through structural modulation from bulk to layered film, Adv. Mater. 29 (2017) 1603157.

[113] P. Vashishtha, M. Ng, S.B. Shivarudraiah, J.E. Halpert, High efficiency blue and green light-emitting diodes using Ruddlesden–Popper inorganic mixed halide perovskites with butylammonium interlayers, Chem. Mater. 31 (2018) 83–89.

[114] C. Qin, T. Matsushima, W.J. Potscavage, A.S.D. Sandanayaka, M.R. Leyden, F. Bencheikh, K. Goushi, F. Mathevet, B. Heinrich, G. Yumoto, Y. Kanemitsu, C. Adachi, Triplet management for efficient perovskite light-emitting diodes, Nat. Photonics 14 (2020) 70–75.

[115] P. Pang, G. Jin, C. Liang, B. Wang, W. Xiang, D. Zhang, J. Xu, W. Hong, Z. Xiao, L. Wang, G. Xing, J. Chen, D. Ma, Rearranging low-dimensional phase distribution of quasi-2D perovskites for efficient sky-blue perovskite light-emitting diodes, ACS Nano 14 (2020) 11420–11430.

[116] Y. Jin, Z.K. Wang, S. Yuan, Q. Wang, C. Qin, K.L. Wang, C. Dong, M. Li, Y. Liu, L.S. Liao, Effects of enrofloxacin and Cu combined pollution on the activities of digestive enzymes of earthworm in soil, J. Appl. Ecol. 30 (2019) 2049–2055.

[117] S. Yuan, Z.K. Wang, L.X. Xiao, C.F. Zhang, S.Y. Yang, B.B. Chen, H.T. Ge, Q.S. Tian, Y. Jin, L.S. Liao, Optimization of low-dimensional components of quasi-2D perovskite films for deep-blue light-emitting diodes, Adv. Mater. 31 (2019) 1904319.

[118] M. Worku, Q. He, L.-j. Xu, J. Hong, R.X. Yang, L.Z. Tan, B. Ma, Phase control and in situ passivation of quasi-2D metal halide perovskites for spectrally stable blue light-emitting diodes, ACS Appl. Mater. Interfaces 12 (2020) 45056–45063.

[119] D. Ma, P. Todorovic, S. Meshkat, M.I. Saidaminov, Y.K. Wang, B. Chen, P. Li, B. Scheffel, R. Quintero-Bermudez, J.Z. Fan, Y. Dong, B. Sun, C. Xu, C. Zhou, Y. Hou, X. Li, Y. Kang, O. Voznyy, Z.H. Lu, D. Ban, E.H. Sargent, Chloride insertion-immobilization enables bright, narrowband, and stable blue-emitting perovskite diodes, J. Am. Chem. Soc. 142 (2020) 5126–5134.

[120] Q. Wang, X. Wang, Z. Yang, N. Zhou, Y. Deng, J. Zhao, X. Xiao, P. Rudd, A. Moran, Y. Yan, J. Huang, Efficient sky-blue perovskite light-emitting diodes via photoluminescence enhancement, Nat. Commun. 10 (2019) 5633.

[121] Z. Chu, Y. Zhao, F. Ma, C.X. Zhang, H. Deng, F. Gao, Q. Ye, J. Meng, Z. Yin, X. Zhang, J. You, Large cation ethylammonium incorporated perovskite for efficient and spectra stable blue light-emitting diodes, Nat. Commun. 11 (2020) 4165.

[122] Y. Liu, J. Cui, K. Du, H. Tian, Z. He, Q. Zhou, Z. Yang, Y. Deng, D. Chen, X. Zuo, Y. Ren, L. Wang, H. Zhu, B. Zhao, D. Di, J. Wang, R.H. Friend, Y. Jin, Efficient blue light-emitting diodes based on quantum-confined bromide perovskite nanostructures, Nat. Photonics 13 (2019) 760–764.

[123] Z. Ren, X. Xiao, R. Ma, H. Lin, K. Wang, X.W. Sun, W.C.H. Choy, Hole transport bilayer structure for quasi-2D perovskite based blue light-emitting diodes with high brightness and good spectral stability, Adv. Funct. Mater. 29 (2019) 1905339.

[124] Y. Shen, K.C. Shen, Y.Q. Li, M. Guo, J. Wang, Y. Ye, F.M. Xie, H. Ren, X. Gao, F. Song, J.X. Tang, Interfacial potassium-guided grain growth for efficient deep-blue perovskite light-emitting diodes, Adv. Funct. Mater. 31 (2020) 2006736.

[125] Y.K. Wang, D. Ma, F. Yuan, K. Singh, J.M. Pina, A. Johnston, Y. Dong, C. Zhou, B. Chen, B. Sun, H. Ebe, J. Fan, M.J. Sun, Y. Gao, Z.H. Lu, O. Voznyy, L.S. Liao, E.H. Sargent, Chelating-agent-assisted control of $CsPbBr_3$ quantum well growth enables stable blue perovskite emitters, Nat. Commun. 11 (2020) 3674.

[126] H.P. Kim, J. Kim, B.S. Kim, H.-M. Kim, J. Kim, A.R.b.M. Yusoff, J. Jang, M.K. Nazeeruddin, High-efficiency, blue, green, and near-infrared light-emitting diodes based on triple cation perovskite, Adv. Opt. Mater. 5 (2017) 1600920.

[127] T. Du, N. Wang, H. Chen, H. Lin, H. He, Comparative study of vapor- and solution-crystallized perovskite for planar heterojunction solar cells, ACS Appl. Mater. Interfaces 7 (2015) 3382–3388.

[128] M. Karlsson, Z. Yi, S. Reichert, X. Luo, W. Lin, Z. Zhang, C. Bao, R. Zhang, S. Bai, G. Zheng, P. Teng, L. Duan, Y. Lu, K. Zheng, T. Pullerits, C. Deibel, W. Xu, R. Friend, F. Gao, Mixed halide perovskites for spectrally stable and high-efficiency blue light-emitting diodes, Nat. Commun. 12 (2021) 361.

[129] Z.J. Yong, S.Q. Guo, J.P. Ma, J.Y. Zhang, Z.Y. Li, Y.M. Chen, B.B. Zhang, Y. Zhou, J. Shu, J.L. Gu, L.R. Zheng, O.M. Bakr, H.T. Sun, Doping-enhanced short-range order of perovskite nanocrystals for near-unity violet luminescence quantum yield, J. Am. Chem. Soc. 140 (2018) 9942–9951.

[130] W. Deng, X. Xu, X. Zhang, Y. Zhang, X. Jin, L. Wang, S.-T. Lee, J. Jie, Organometal halide perovskite quantum dot light-emitting diodes, Adv. Funct. Mater. 26 (2016) 4797–4802.

[131] F. Zhang, B. Cai, J. Song, B. Han, B. Zhang, H. Zeng, Efficient blue perovskite light-emitting diodes boosted by 2D/3D energy cascade channels, Adv. Funct. Mater. 30 (2020) 2001732.

[132] F. Zhang, X. Zhang, C. Wang, M. Sun, X. Luo, Y. Yang, S. Chang, D. Zhang, L. Duan, Chlorine distribution management for spectrally stable and efficient perovskite blue light-emitting diodes, Nano Energy 79 (2021) 105486.